[Papers in Palaeontology, 2023, e1531]

Three-dimensional reconstruction, taphonomic and petrological data suggest that the oldest record of bioturbation is a body fossil coquina

by CHRISTOS PSARRAS[1,7,*], PHILIP C.J. DONOGHUE[1], RUSSELL J. GARWOOD[2,3], DMITRIY V. GRAZHDANKIN[4], LUKE A. PARRY[5], VLADIMIR I. ROGOV[4] *and* ALEXANDER G. LIU[6,*]

[1]Bristol Palaeobiology Group, School of Earth Sciences, University of Bristol, Life Sciences Building, 24 Tyndall Avenue, Bristol BS8 4QQ, UK; philip.donoghue@bristol.ac.uk
[2]Department of Earth & Environmental Sciences, The University of Manchester, Manchester M13 9PL, UK; russell.garwood@manchester.ac.uk
[3]Natural History Museum, London SW7 5BD, UK
[4]Trofimuk Institute of Petroleum Geology & Geophysics, Koptyug Avenue 3, Novosibirsk 630090, Russia; dima.grazhdankin@gmail.com, rogovvi@ipgg.sbras.ru
[5]Department of Earth Sciences, University of Oxford, South Parks Road, Oxford OX1 3AN, UK; luke.parry@earth.ox.ac.uk
[6]Department of Earth Sciences, University of Cambridge, Downing Street, Cambridge CB2 3EQ, UK; agscl2@cam.ac.uk
[7]*Current address:* Department of Historical Geology–Paleontology, Faculty of Geology & Geoenvironment, National & Kapodistrian University of Athens, 15784 Zografou, Panepistimiopolis, Greece; cpsarras@geol.uoa.gr
*Corresponding author

Typescript received 22 December 2022; accepted in revised form 1 August 2023

Abstract: Fossil material assigned to *Nenoxites* from the late Ediacaran Khatyspyt Formation of Arctic Siberia (550–544 Ma) has been presented as evidence for bioturbation prior to the basal Cambrian boundary. However, that ichnological interpretation has been challenged, and descriptions of similar material from other global localities support a body fossil origin. Here we combine x-ray computed tomography, scanning electron microscopy and petrographic methods to evaluate the body or trace fossil nature of *Nenoxites* from the Khatyspyt Formation. The fossilized structures consist of densely packed chains of three-dimensionally preserved silicic, bowl-shaped elements surrounded by distinct sedimentary halos, in a dolomitized matrix. Individual bowl-shaped elements can exhibit diffuse mineralogical boundaries and bridging connections between elements, both considered here to result from silicification and dolomitization during diagenesis. This new morphological and petrological evidence, in conjunction with recent studies of the late Ediacaran tubular taxa *Ordinilunulatus* and *Shaanxilithes* from China, suggest that the Khatyspyt specimens most probably reflect a coquina deposit of *Shaanxilithes*-like body fossils. Our data support the possibility of *Shaanxilithes*-like organisms representing total group eumetazoans.

Key words: Ediacaran, sedimentology, taphonomy, *Nenoxites*, bioturbation, petrology.

PHYLOGENETIC studies predict a Neoproterozoic origin for Metazoa tens of millions of years prior to the start of the Cambrian, and imply that the stem groups of most bilaterian phyla originated during the Ediacaran Period (635–539 Ma) (e.g. Erwin *et al.* 2011; dos Reis *et al.* 2015). Although often contentious (Cunningham *et al.* 2017), claims for body fossils of animals from the late Ediacaran Period (*c.* 574–539 Ma) have been bolstered by recent discoveries, analyses and developmental data, which together support the presence of total group (e.g. Liu *et al.* 2014; Evans *et al.* 2017; Cai *et al.* 2019; Dunn *et al.* 2019, 2021) and crown-group (Dunn *et al.* 2022) eumetazoans by the middle Ediacaran, as well as candidate bilaterians in Ediacaran fossil assemblages younger than *c.* 558 Ma (e.g. Fedonkin & Waggoner 1997; Gold *et al.* 2015; Evans *et al.* 2020; Willman & Slater 2021).

Trace fossils, which record the activity or behaviour of an organism, offer an independent record of metazoan evolution across the Ediacaran–Cambrian interval (Seilacher 1989; Budd & Jensen 2000; Buatois & Mángano 2016), with horizontal surface traces at 565 Ma being the oldest candidate total group eumetazoan traces (Liu *et al.* 2010; age constrained by Matthews *et al.* 2021). Meanwhile, systematic burrowing behaviour documented by earliest Cambrian ichnofossils has been considered to record the ecological transition from Ediacaran 'matgrounds' to Phanerozoic 'mixgrounds', revolutionizing sediment burial processes and nutrient cycling (e.g. McIlroy & Logan 1999; Bottjer *et al.* 2000; Buatois &

doi: 10.1002/spp2.1531

Mángano 2011; Mángano & Buatois 2017, 2020; Tarhan 2018). The first appearance of the ichnofossil *Treptichnus pedum* is inferred to document a globally synchronous radiation of a specific complex burrowing behaviour, and defines the base of the Cambrian System (Brasier *et al.* 1994). However, a range of late Ediacaran trace fossils, comprising surficial or shallow horizontal burrows from nearshore marine settings younger than *c.* 555 Ma appear to be a prelude to Cambrian burrowing activity (e.g. Carbone & Narbonne 2014; Chen *et al.* 2018, 2019; Gehling & Droser 2018; Xiao *et al.* 2019; Darroch *et al.* 2021). Structures interpreted to record vertical 'shuffling' through sediment occur at *c.* 560 Ma (Menon *et al.* 2013), while latest Ediacaran strata contain meiofaunal burrows (Parry *et al.* 2017; Darroch *et al.* 2021), probing vertical traces produced by priapulid-like behaviour (e.g. Tarhan *et al.* 2020; Darroch *et al.* 2021; Turk *et al.* 2022), and very shallow burrows (e.g. Buatois & Mángano 2011; Meyer *et al.* 2014; Darroch *et al.* 2021). Many of these examples have been considered to record the activity of bilaterian organisms, but Ediacaran evidence of two other common products of bilaterian behaviour (not necessarily unique to bilaterians), vertical meniscate sediment-penetrative burrowing and bioturbation, is typically rare or controversial (Macdonald *et al.* 2014; Mángano & Buatois 2014; Buatois & Mángano 2016; Tarhan *et al.* 2020).

Material described from the *c.* 550–544 Ma Khatyspyt Formation of Siberia (Sokolov & Fedonkin 1984; Fedonkin 1988; Rogov *et al.* 2012, 2013a, 2013b; Cherry *et al.* 2022) is of critical importance for understanding the timing and nature of both behavioural innovation and metazoan evolution more broadly. Fossil material assigned to the ichnogenus *Nenoxites* Fedonkin, 1976, by Rogov *et al.* (2012) was interpreted by those authors as evidence for burrowing involving meniscate backfilling, on the basis of taphonomic, palaeoecological and sedimentological lines of observation. That evidence includes morphologies consistent with phobotaxis (Rogov *et al.* 2013a) and vertical escape behaviour, the absence of branching, disturbance of primary lamination, secondary erosion of candidate meniscae by subsequent sedimentary deposits, and the presence of connective structures reminiscent of mucus-wall drains (Rogov *et al.* 2012). Such an interpretation would extend the ichnofossil record of bilaterians capable of producing complex backfill burrow structures (and thus their associated impact on sediments), by *c.* 10 myr (Mángano & Buatois 2020; Tarhan *et al.* 2020; Darroch *et al.* 2021).

The ichnological interpretation of the Khatyspyt material has been challenged by suggestions that it may instead represent the body fossil remains of tubular organisms (Brasier *et al.* 2013). Other researchers accept that the material may document bioturbation, but by mycetozoan amoebozoans rather than by metazoans (Gámez Vintaned & Zhuravlev 2013). Over the past two decades, similar material from Siberia, Ukraine, China, India and Namibia (e.g. Shen *et al.* 2007; Dong *et al.* 2008; Zhuravlev *et al.* 2009; Meyer *et al.* 2012; Rogov *et al.* 2013a, 2013b; Tarhan *et al.* 2014; Darroch *et al.* 2016; Wood *et al.* 2017; Zhu *et al.* 2017; Ivantsov 2018; Luo & Miao 2020; Liu *et al.* 2022; Yi *et al.* 2022) has been described, offering multiple points of comparison. Concurrently, meticulous study of extensive collections of the body fossil *Shaanxilithes* Xing *et al.*, 1984, a potential index fossil for latest Ediacaran strata (e.g. Meyer *et al.* 2012; Chai *et al.* 2021), has identified multiple taphonomic modes for *Shaanxilithes* preservation (Wang *et al.* 2021), some of which bear strong resemblance to the Siberian *Nenoxites* material (similarities between some *Nenoxites* and *Shaanxilithes* specimens were also recognized by Meyer *et al.* 2012, Ivantsov 2018 and Rogov *et al.* 2012, while more recently *Nenoxites* and certain *Palaeopascichnus* specimens from South China have been considered to reflect taphonomic variants or closely related taxa; Luo & Miao 2020; Yi *et al.* 2022; although see also Liu *et al.* 2022).

Here we reanalyse the Khatyspyt Formation *Nenoxites* material in an attempt to discriminate between body and trace fossil interpretations. Digital reconstruction of the preserved structures from computed tomography (CT) scans permits visualization of their three-dimensional (3D) morphology. Optical microscopy and scanning electron microscopy (SEM) studies elucidate the taphonomic and diagenetic history of the material, and provide insight into its formation. Our results permit both re-evaluation of the trace fossil interpretation proposed for this material, and direct comparison of the Khatyspyt Formation material with similar, broadly coeval, body fossil material.

GEOLOGICAL SETTING

The fossiliferous Khatyspyt Formation of the late Ediacaran Khorbusuonka Group reaches 245 m in thickness and consists of alternating thin limestones and shales, finely laminated thin- to medium-bedded limestones, planar- to wavy-laminated thick-bedded limestones, and intraclastic dolomitized limestones occurring as laterally persistent channelized deposits over tens to hundreds of metres, all punctuated by thin interbeds of volcanic tuff and packages of shales. Sedimentological observations suggest deposition in a starved intracratonic rift basin developed in a marine inner-ramp setting influenced by wave and current activity, with intraclastic limestones representing debris flows deposited adjacent to inferred syn-sedimentary faults (Knoll *et al.* 1995; Pelechaty *et al.* 1996; Nagovitsin *et al.* 2015; Kolesnikov *et al.* 2018).

The Khatyspyt Formation hosts a considerable diversity of macrofossil impressions of soft-bodied candidate animals (including rangeomorphs and arboreomorphs), carbonaceous compression fossils (mega-algae), and trace fossils (Sokolov & Fedonkin 1984; Vodanjuk 1989; Fedonkin 1990; Grazhdankin *et al.* 2008; Nagovitsin *et al.* 2015; Bykova *et al.* 2017, 2020), in addition to organic biomarkers (Duda *et al.* 2016, 2020). Fossil distribution is controlled by lithofacies. The meniscate structures described herein are confined to a facies that is in close proximity to carbonaceous compression macrofossils (although never on the same surfaces), but is otherwise devoid of macrofossils.

The studied material was collected from finely laminated silicified and dolomitized mudstones in the uppermost part of Member 3 of the Khatyspyt Formation (Nagovitsin *et al.* 2015, section 0602), cropping out at the mouth of Anabyl Creek, left tributary of the Khorbusuonka River, Olenek Uplift, Republic of Sakha, Siberia, Russia (Fig. 1A). Extensive regional silicification in the uppermost beds of Member 3 is attributed to the presence of thin, devitrified volcanic tuff interbeds. A diatreme dated to 543.9 ± 0.3 Ma (the Tas-Yuryakh volcanic complex; Bowring *et al.* 1993) penetrates the Khatyspyt Formation as well as the overlying Turkut Formation and lowermost part of the Syhargalakh Formation, providing a minimum age constraint for the material under study (Fig. 1; Rogov *et al.* 2012; Nagovitsin *et al.* 2015). A maximum age constraint of 550 Ma is provided by a detrital zircon U–Pb isotopic age from the top of the underlying Maastakh Formation (Cherry *et al.* 2022).

The studied horizons are part of a 2.64-m-thick fining-upward package consisting of planar- and hummocky-stratified pelsparite, overlain by a succession of alternating finely laminated sparite and micrite interbeds. The finely laminated limestone interbeds are characterized by erosive bases and flat tops. Erosional scours cut down to a depth of up to 17 mm and are filled with finely laminated limestone (Fig. 1C, D). The upper part of limestone interbeds can consist of densely packed meniscate structures that occasionally become selectively silicified (Fig. 1C). An interval of 17.23 m logged in the upper part of Member 3 of the Khatyspyt Formation consists of 17 such packages of different thickness.

The studied sample is a 50-mm-thick bed originating from one of these partly silicified limestone interbeds, and was collected from a horizon 26.77 m from the base of the section (Figs 1C–E, 2). The bed has an erosive base, which cuts down to a depth of up to 11 mm into the underlying fossil-bearing stratum (best seen at left in Fig. 2A, also magnified in Rogov *et al.* 2012, fig. 1A–B). The scour was initially filled by finely laminated limestone that does not contain fossils (Fig. 1C; 'dark layer' in Fig. 2B; see also Rogov *et al.* 2012, fig. 1A–B). The fossil material is confined to the upper portion of the studied stratum (Fig. 2), and gives the appearance of being inverse graded, with larger elements being located towards the top of the bed. The top of the studied stratum has been scoured (Fig. 2B, also magnified in Rogov *et al.* 2013a, fig. 1A). In the studied sample, fossils are preserved three-dimensionally, although elsewhere in the Khatyspyt Formation similar structures can manifest as low hypo- or epirelief on the sediment surface (Rogov *et al.* 2012, fig. 3). The figured beds are interpreted to have been deposited in a shallow marine storm-influenced environment on a carbonate ramp (Duda *et al.* 2020).

MATERIAL AND METHOD

A triangular block of the fossil-bearing horizon (CAMSM X 50382.1; lateral dimensions: 6.30 cm, 5.50 cm and 5.42 cm, height: 3.10 cm) (Figs 1C, 2D) was scanned using x-ray microtomography (μCT) at the Natural History Museum in London with a Nikon Metrology HMX ST 225 instrument. X-rays were generated using a tungsten target, with an accelerating voltage of 180 kV, a current of 140 μA, and no filtration. A total of 3142 projections were collected with a 708 ms exposure, and reconstructed to a create a 33.7 μm voxel size volume. In order to explore the data, the 32-bit floating point volume was loaded in Drishti import v2.5.1 (Limaye 2012), then windowed and the histogram stretched around the grey levels of the sample. Data were exported as an 8-bit PNG stack. This stack was then imported into SPIERSedit v2.2.0 (Sutton *et al.* 2012). The low attenuation contrast of the scan coupled with the density of the rock resulted in beam hardening artefacts (i.e. the greyscale values for each phase were darker inside the sample). These were minimized by creating broadly circular regions of interest in the sample, and applying different linear threshold values to each. From these thresholds, a surface was exported to SPIERSview v2.2.0, and the smallest islands were removed (object, island removal, tiny). The resulting mesh was then exported and then imported into Blender v2.79 (see Garwood & Dunlop (2014) for an overview), in which mesh islands were separated for individual inspection following the methodology outlined in Parry *et al.* (2017). This provided an overview of the morphology. However, the low contrast, the beam hardening and the presence of diagenetically introduced crystals of different densities inside the specimens, coupled with differential compaction of individual elements, hampered attempts to identify precise fossil outlines in the μCT slice data. These factors precluded the tracing of individual chains of elements through the slab. As such, the specimens

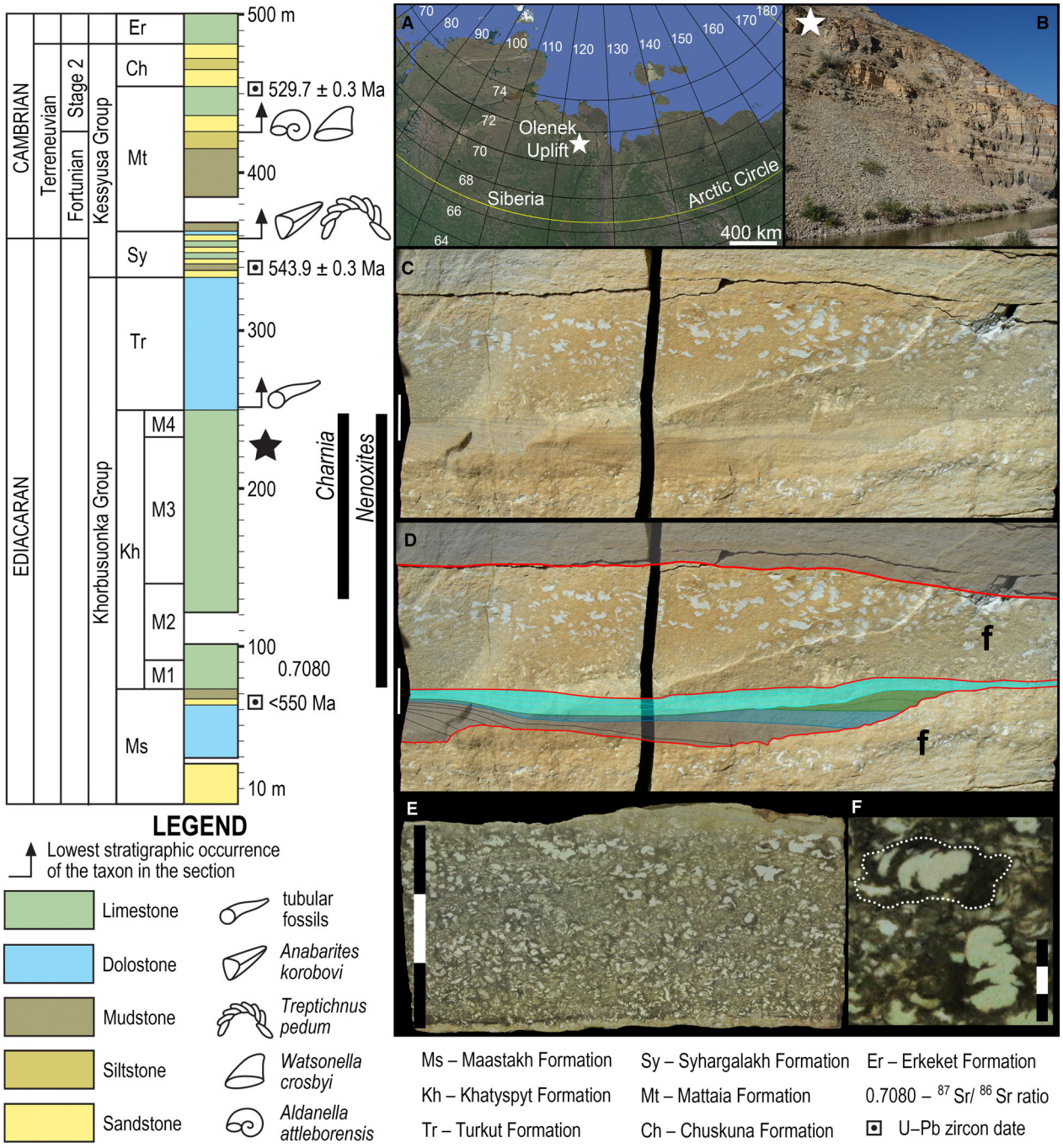

FIG. 1. Stratigraphic, geographical and geological context for the studied material. A, location of the field area in northern Siberia (Russia) (star). B, the Anabyl Creek section along the left tributary of the Khorbusuonka River (lat. 71.200625, long. 123.726222 in WGS84 datum), with the fossil-bearing strata indicated towards the top of the section (star). C–D, close-up view of two fossiliferous horizons (f) delineated by erosional surfaces (bold red lines); note that the scour at the base of the upper fossil-bearing bed has initially been filled by cross-bedded and then planar-laminated sediment (coloured in D), which is devoid of fossils. E, polished slab of the studied material (CAMSM X 50382.1). F, close-up view of E, showing the halo boundaries surrounding a series. Scale bar lengths/divisions represent 1 cm (C–E). Stratigraphy follows Nagovitsin *et al.* (2015).

presented here were traced by following the trajectory of the elements in AVIZO v8 and searching for other elements in close proximity. If multiple elements were nearby (a frequent situation), the surrounding series were also traced, enabling us to manually assign elements to the correct series.

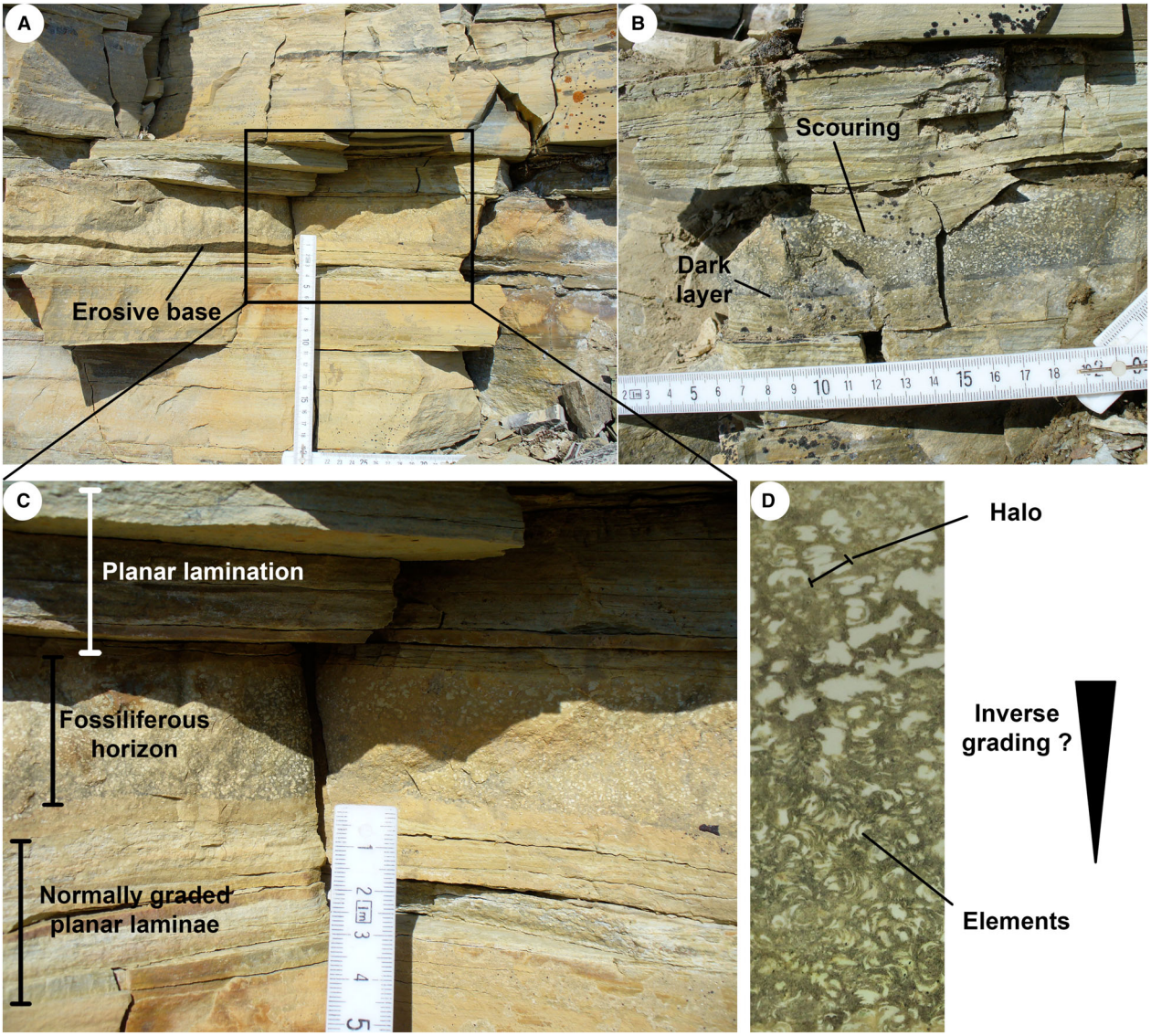

FIG. 2. *In situ* sedimentological context of the studied material from the Khatyspyt Formation. A, general view of the sedimentology at the mouth of Anabyl Creek, Khorbusuonka River, Siberia; the undulating erosive base of the fossil-bearing bed is highlighted in dark brown. B, scouring of the fossil bed by overlying deposits; the fossils themselves are truncated by scours in some places; note the dark layer possessing internal lamination in the lowest millimetres of the fossil-bearing bed. C, sedimentology immediately surrounding the fossil-bearing horizon (which appears to have smaller fossil elements towards the base of the bed and larger elements towards the top). D, close-up view of the fossil-bearing horizon showing 'series' of pale green 'elements' surrounded by dark, olive-green 'halos'; variation in the size of elements through the bed is indicated, and could be interpreted as evidence for inverse grading if the elements were originally particles deposited in the sediment; alternatively, the variation in size may reflect a progressive increase in the amount of diagenetic overgrowth of silicic material towards the top of the bed (discussed in the text). Ruler has mm and cm increments.

Thin sections cut perpendicular to bedding through the Siberian material (CAMSM X 50382.2.1 to CAMSM X 50382.4.1) were carbon-coated and analysed using a Hitachi S3500-N scanning electron microscope with a silicon drift detector at the School of Earth Sciences, University of Bristol. Crystal chemistry and element maps were acquired using energy dispersive spectroscopy at 15 kV, and a working distance of either 15 or 20 mm. Weight percent elemental maps were generated using standardless quantification (i.e. all count totals were normalized to 100%). The hand specimen and thin sections are accessioned in the Sedgwick Museum, University of Cambridge, UK (CAMSM). All raw files relating to µCT scans, tomographic reconstruction, and SEM are stored in the Bristol Data Repository (Psarras *et al.* 2023).

RESULTS

Three-dimensional reconstruction

Three-dimensional reconstruction of the Khatyspyt material from μCT data shows multiple bowl-shaped structures, here termed 'elements' (referred to as 'intervening menisci' by Rogov *et al.* 2012, and comparable to the 'crescentic segments' or 'internal nested tubes' of Wang *et al.* 2021, and 'dishes' of Liu *et al.* 2022), serially arranged in 'series' (i.e. the 'strings' in Liu *et al.* 2022) (Figs 3, 4). Note that the packages of sediment occurring between these bowl-shaped structures were described as 'menisci' by Rogov *et al.* (2012). Each series of elements is enclosed in a distinct cylindrical–elliptical region of sediment of slightly different colour and mineralogical composition to the surrounding substrate, here termed a 'halo' (Figs 1F, 2D, 3E). This halo is equivalent to that described by Rogov *et al.* (2012, fig. 3), who interpreted it as a diagenetic artefact of silicification, and also to halos described in the Chinese taxon *Ordinilunulatus* by Liu *et al.* (2022, fig. 7), who interpreted it as a biological structure. The width of the surrounding halo remains constant throughout a series (Fig. 3E, see also Rogov *et al.* 2013b, fig. 1c), but halos can be of variable clarity, with some being almost impossible to distinguish from other halos or the substrate, while others, typically surrounding large, well-defined series, have sharp boundaries (e.g. Fig. 2D).

Digital reconstruction of 55 series shows that the elements constituting individual series are consistent in shape and size (Fig. 3). Individual series have broadly consistent element length and length : width ratios (ratios range from 1 to 2; Fig. 5A), with elements from different series measuring 0.63–2.55 mm in length and 0.37–1.85 mm in width (n = 151 measured elements). Although the elements are reasonably uniform in shape (mean length : width ratio = 1.52, mode = 1.5, Fig. 5), extreme ratios (min. = 1, max. = 3.48) are observed (Fig. 5A, outlier elements). Series are not observed to branch, and do not cross-cut one another in three dimensions. Adjacent elements in a series can be in direct contact, or separated by distances of up to 0.42 mm (Fig. 4). Most digitally reconstructed specimens have a thin, thread-like connection between adjacent elements (248 of 253 observed elements), here termed a 'bridge' (*sensu* Brasier *et al.* 2013; referred to as a 'connection' in *Ordinilunulatus* by Liu *et al.* 2022), but in the Khatyspyt material this bridge is not consistently positioned with respect to the centre of the elements, and its length and width are variable even in individual series (Figs 3, 4). Importantly, when a bridge is observed, its size is considerably greater than the voxel size for the CT scans, suggesting that the absence of such structures between some elements is a genuine absence rather than an artefact of the resolution of the CT data. Individual series follow a variety of 3D trajectories at all angles to the bedding surface, including straight and sub-vertically aligned series, as well as examples that change direction by up to 180° (Fig. 3F). The maximum observed change in angle between two consecutive elements is 50°. Most individual series eventually collide with other specimens when tracked through the sample, preventing conclusive determination of whether they possess distinct terminal morphologies (see the full sample image mesh in the Data Repository). The longest measured individual series contained 31 elements. Examples of isolated elements, not in obvious association with any neighbouring series, were also observed. No obvious, consistently shaped terminal structure was observed in the studied population.

Petrology and SEM

Optical microscopy and SEM analyses confirm a largely dolomitic composition for both the sedimentary matrix and the halos. Micron-scale angular rhombs of sucrosic dolomite, often with clear compositional zoning (Fig. 6F), comprise *c.* 70% of the matrix, with the remainder composed of feldspars, quartz and minor pyrite grains (Fig. 6). This mineralogical composition is confirmed by elemental mapping of the sample (Fig. 7), which indicates the presence of dolomite (areas of enrichment in Ca, Mg) (Fig. S1), quartz (Si) and feldspars (Al, K). Notably, the halo shows little compositional difference to the surrounding sediment: there appears to be slightly more dolomite (Ca and Mg in the elemental maps) with respect to silica in the halo (Fig. 7), but this perception may result from differences in grain size rather than composition. In contrast, the fine-grained material comprising the bowl-shaped elements is largely silicic (Fig. 6), with occasional larger crystals of intergrown dolomite and calcite, the latter inferred to have formed during late-stage diagenesis as a void infill (e.g. Fig. 6E). Dolomite rhombs infiltrate the silicic bowl-shaped elements at their margins, producing a boundary between these elements and surrounding sediment that is diffuse rather than sharp (Fig. 6D). Silicic material compositionally identical to that in the bowl-shaped elements is present between dolomite crystals in both the halos and the surrounding sediment (Fig. 7).

DISCUSSION

Interpretation of the material examined

Petrological analysis of the Khatyspyt Formation material confirms the dolomitic composition of the matrix and the silicification of incorporated elements, as recognized

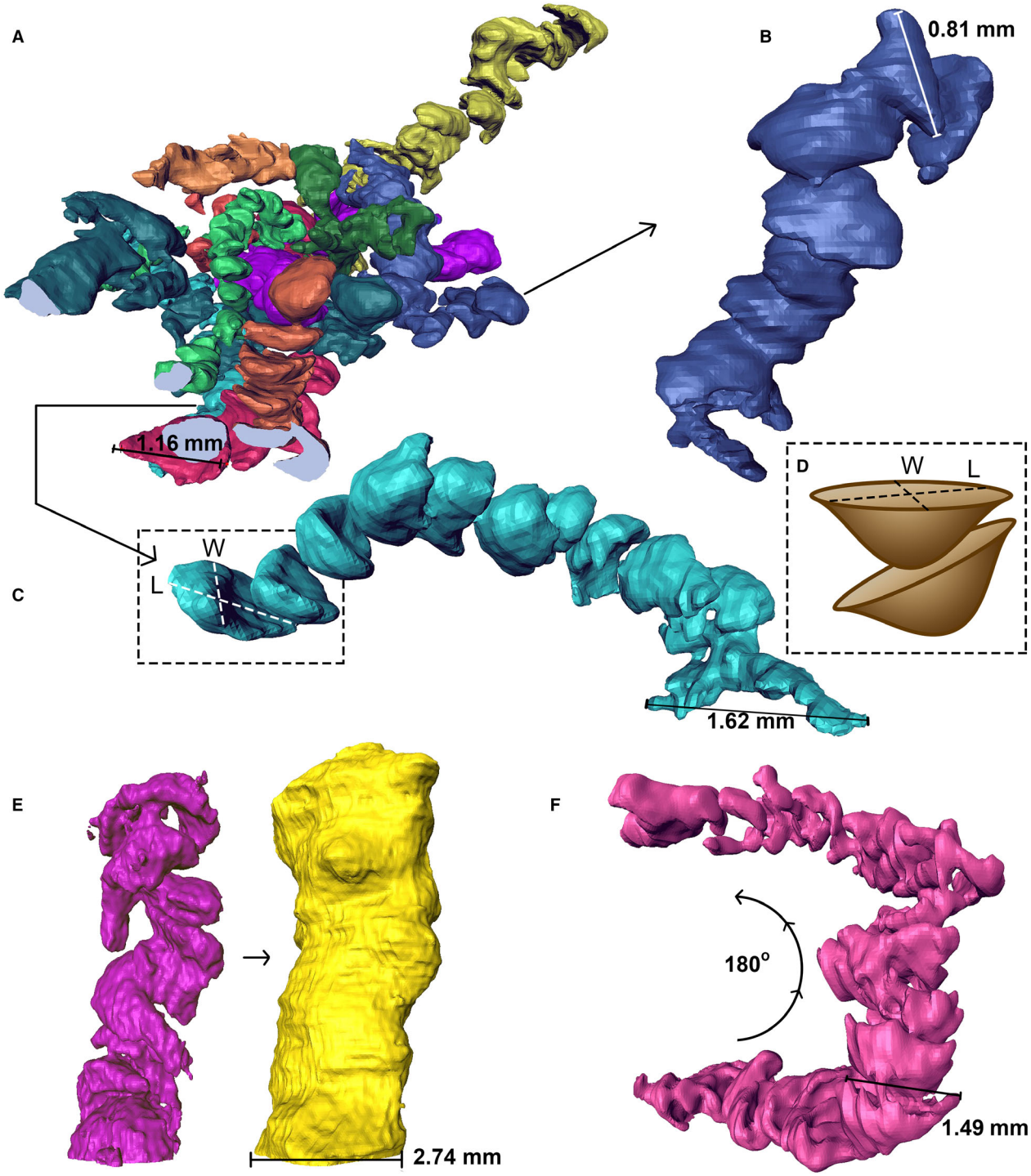

FIG. 3. 3D digital reconstructions of *Nenoxites* specimens from the Khatyspyt Formation. A, group of 11 densely packed series of elements. B, one individual series, consisting of 10 elements. C, individual series of 12 bowl-shaped elements. D, sketch showing how the measurements of length 'L' and width 'W' were extracted from individual elements of the boxed area of series C. E, a single specimen, without (left), and with (right) its associated halo of broadly constant width. F, a series presenting an overall 180° change in direction. Scale bars denote the maximum width of individual elements (A–C, E) or halo (E).

by Rogov *et al.* (2013b). We also recognize a late-stage void-filling crystallization event that has overprinted some of the silicic elements (Fig. 6E). Clearly the specimens have undergone a complex taphonomic history, and we concur with previous authors that diagenetic silicification is likely to be responsible for the diffuse boundaries and

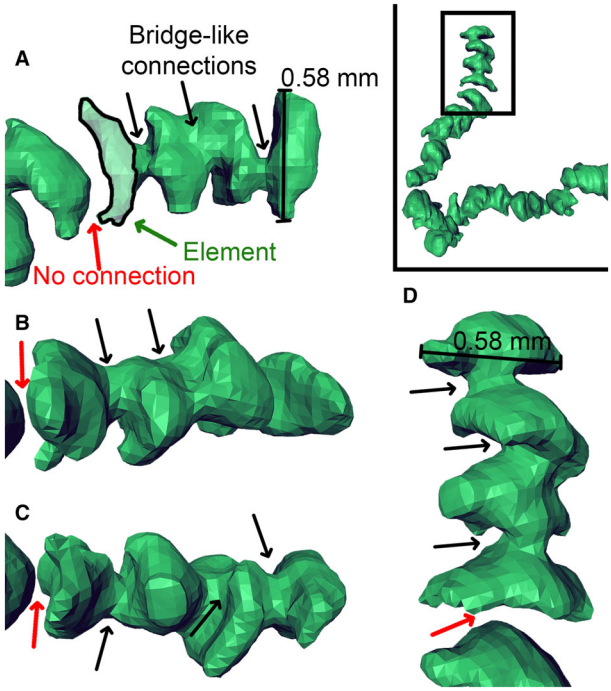

FIG. 4. A–D, views from different angles of a sub-set of elements from a single series (broader context seen at top right), showing their bowl-shaped morphology (e.g. outlined element in A, indicated by the green arrow), the bridge-like connections between elements (black arrows), and examples of non-connected pairs of elements (red arrows). Scale bars indicate the maximum width of the terminal element. Note that individual elements in this single series are of similar size, while connections between elements are not consistent in size, shape or position.

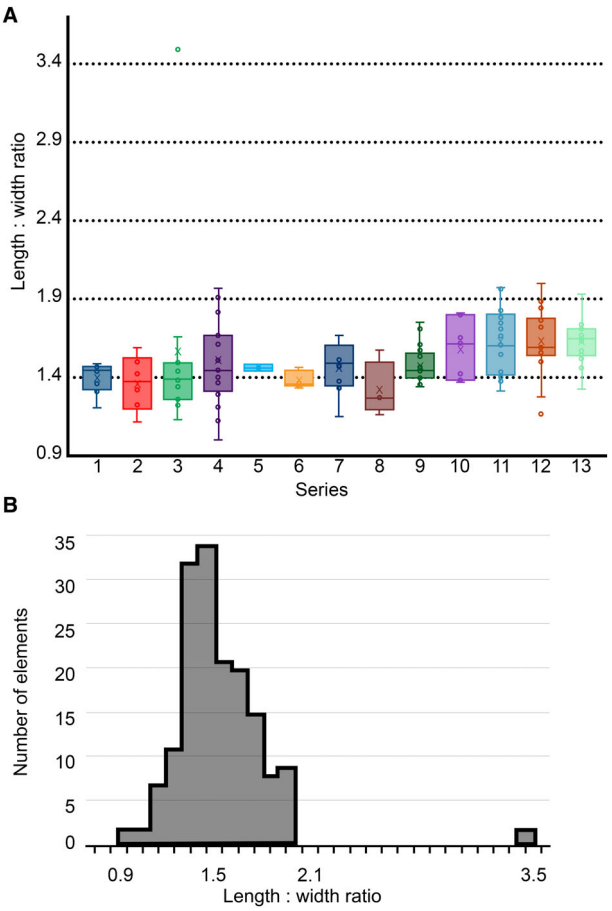

FIG. 5. A, length : width ratio of elements in 13 thirteen reconstructed series; note that the means range between 1.3 and 1.65 (mean = 1.52), indicating that the mean length of each element is *c.* 1.5-fold larger than its width; whiskers represent the lower and upper limits of the data from individual elements in each series, with outlier points visible in two cases (series 3 and 12). B, frequency distribution of the length : width ratios of 151 individual elements; the distribution is positively skewed (2.92) and exhibits positive kurtosis (20.3); most elements have a length : width ratio of between 1.3 and 1.7.

irregular shape of many individual elements and series (e.g. Rogov *et al.* 2013b). An originally biomineralized structure would not be expected to possess an infill of randomly arranged micro- and meso-quartz crystals, and therefore we can discount primary silica biomineralization as an explanation for the elements. Given the propensity for dolomite to form late-stage diagenetic destructive replacement textures (as seemingly evidenced here by its overgrowth of silicic material in the matrix; Fig. 6F), and the observed incursion of dolomite crystals into the silicic elements (Fig. 6D), we infer that silicification of this material occurred early, with dolomitization of the matrix taking place at a later stage in the burial history. This inferred early silicification event is probably the result of devitrification of local tuffs in the Khatyspyt Formation, but is consistent with the association of other global occurrences of *Nenoxites*-like material with silica (although we note that several of those fossils also have associations with clay minerals; e.g. Dong *et al.* 2008; Luo & Miao 2020; Yi *et al.* 2022).

Morphologically, the structures are composed of concavo-convex elements arranged in stacked series, with frequent thread-like connections (Fig. 3), all enveloped in a cylindrical halo (Fig. 3E). The precise width and morphology of the halo cannot always be identified due to interaction with neighbouring series and conflation by diagenetic alteration, but the width of elements in individual series is relatively consistent, while different series have a range of widths (Fig. 5A). Elements possess similar length : width ratios of *c.* 1.5 across the studied population (Fig. 5B).

Importantly, we recognize that the prominent halos surrounding the elements (most clearly observed in the studied hand specimen as a darker green rim around the elements) possess the same mineralogy as the surrounding sedimentary matrix (Fig. 7). If halos reflect a biological or

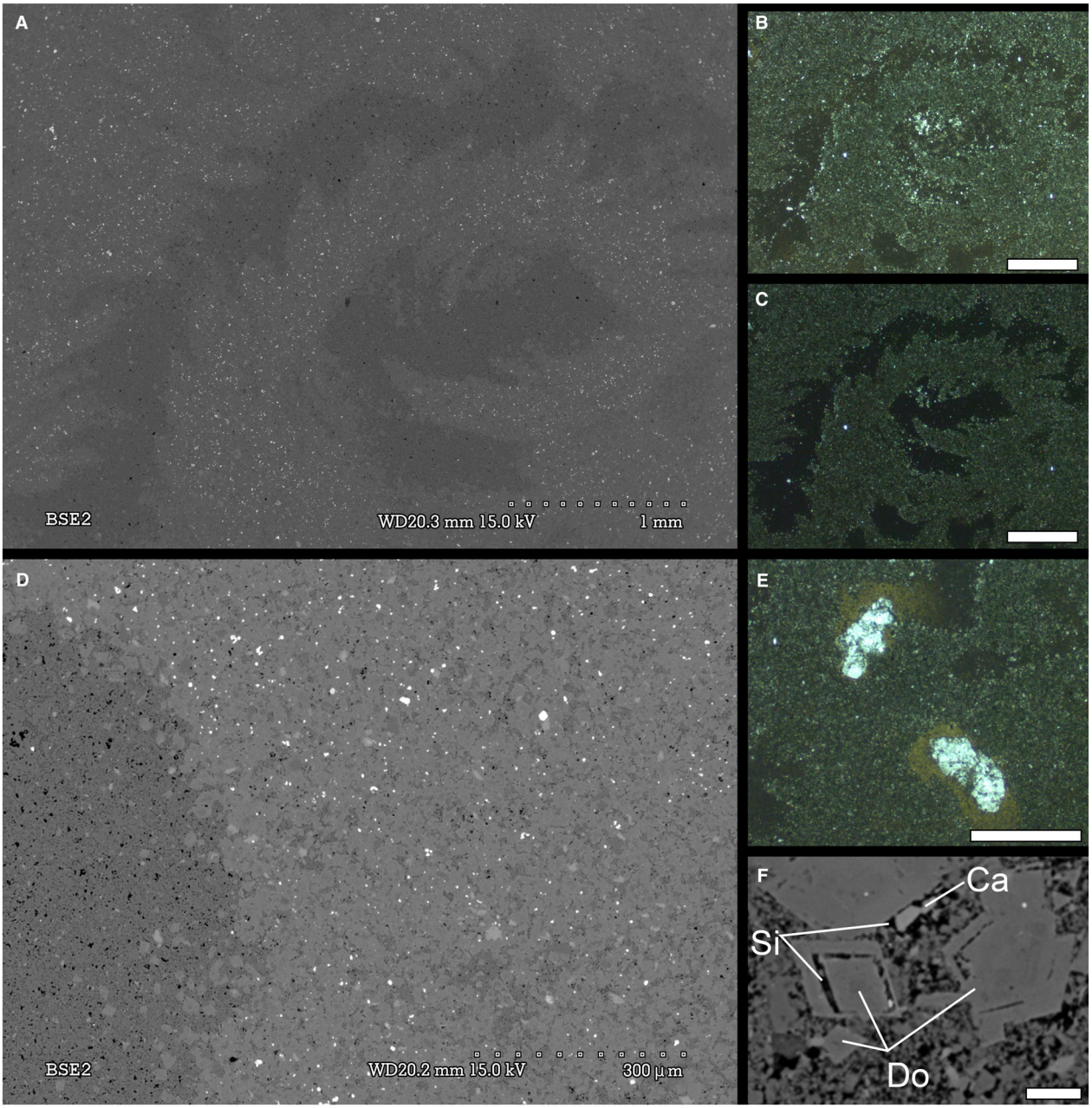

FIG. 6. SEM and light microscopy of the Khatyspyt Formation material in thin section CAMSM X 50382.2.1. A, SEM backscatter; B, optical microscopy plane-polarized; C, optical microscopy cross-polarized views of two series of elements. D, close up SEM backscatter image of the diffuse, irregular margin of an element (left), showing the presence of isolated rhombic dolomite crystals (light grey) in the element. E, cross-polarized optical microscopy image of a series with a large, mineralized vug of calcite and dolomite replacing some of the elements (centre). F, zoning in dolomite crystals in the matrix, which seem to have overgrown or truncated pre-existing calcite and silicate minerals. Scale bars represent: 1 mm (B, C); 0.5 mm (E); 0.01 mm (F).

biologically induced feature, they probably had a distinct original composition relative to the elements they encompass, in order to explain their differential preservation (with the elements having been entirely silicified and then largely unaffected by later dolomitization). True burrow meniscae would be assumed to comprise packages of sediment (potentially of the same, or different, composition to the surrounding matrix), and the organic-rich sediment between such true meniscae could feasibly undergo preferential silicification (Butts 2014). Alternatively in a body fossil model, the halos and elements may originally have been constructed of different biological

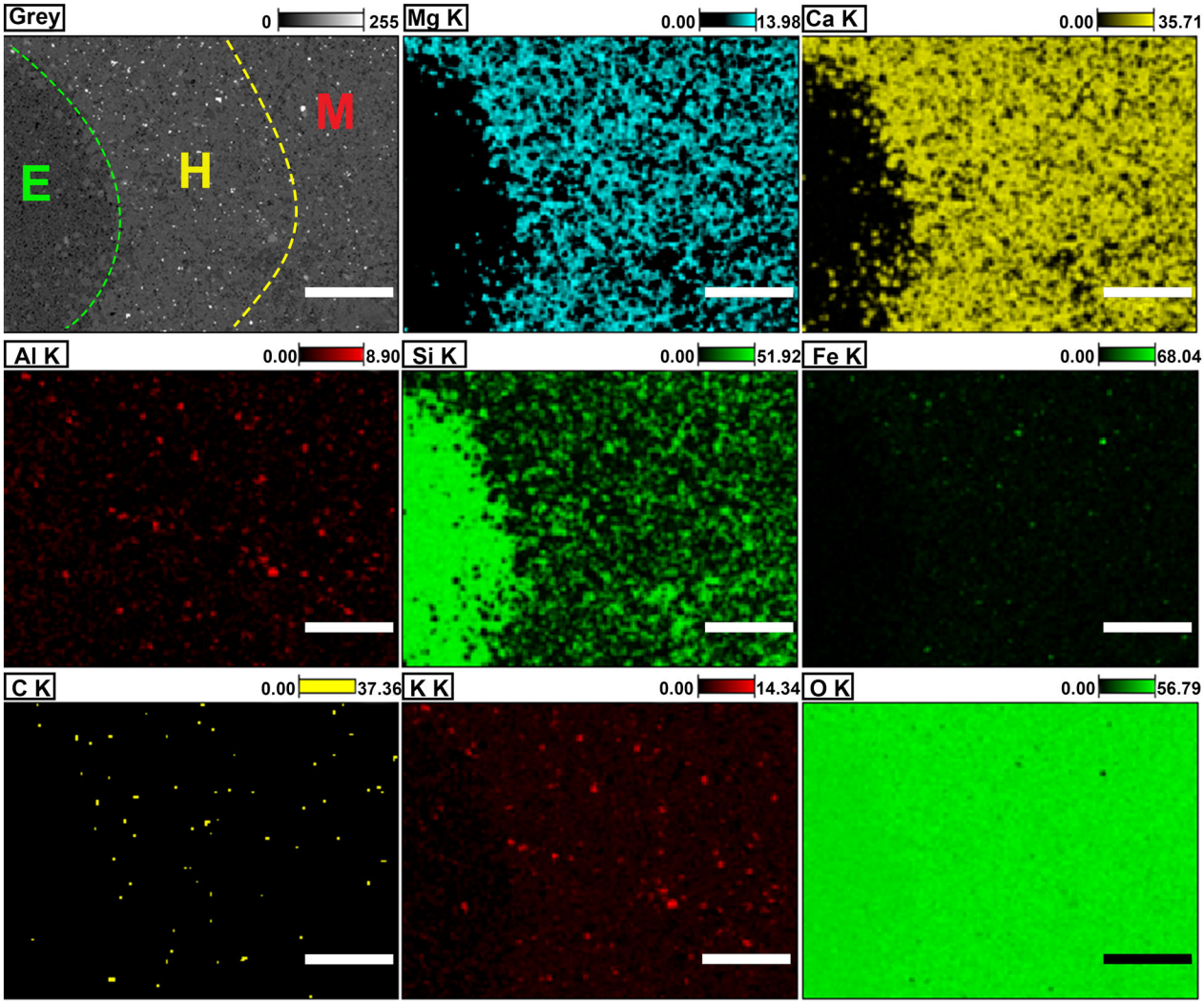

FIG. 7. Elemental maps showing the margin of an element and the surrounding sedimentary matrix. The yellow dashed line in the top left image indicates the boundary between halo (H) and matrix (M); the green dashed line reflects the boundary between element (E) and halo. There is little dolomite or calcite inside the elements (as indicated by the Ca and Mg maps). Silica (Si map) is abundant inside the elements, but also common in patches throughout the halo and matrix. Outside the element, K-feldspars are highlighted by the Al and K maps, and rare probable iron sulfides are shown by the Fe and O maps (i.e. the oxygen-poor regions in the latter). Colour brightness reflects elemental weight percentage per pixel. All scale bars represent 200 μm.

materials, or they could result from decay or diagenetic processes during lithification. Early diagenetic microcrystalline silicification of the elements, removing any available pore space inside them, is our favoured explanation for the observed mineralogical distinction, but it is not exclusive to a trace fossil interpretation. It is also possible that the relative depletion of silica in the halos results from the dissolution and removal of pre-existing siliceous material from those areas during silicification of the elements (promoted by organic matter in the elements), although it is difficult to distinguish between these possibilities from the available data. In all scenarios, silicification of the elements would have been followed by dolomitization of both the sedimentary matrix and the halos (Fig. S2).

The Khatyspyt material can be compared with Upper Cretaceous cherts of the Ekofisk Formation ('Fabric II' of Blinkenberg *et al.* 2021), which formed via progressive silica replacement interspersed with calcite recrystallization (Blinkenberg *et al.* 2021). Such cycles of silica dissolution and recrystallization could have filled voids between original calcite crystals and created voids inside individual elements, which could then be filled by later precipitation of calcite to produce the observed carbonate fabrics. In this model, either silicification or recrystallization could have produced the diffuse element boundaries we observe, as

well as the irregular shapes of the elements (Fig. 5), the inconsistent appearance and placement of bridging structures, and the variable clarity of the halos (Fig. 2D). In sum, our taphonomic data suggest that the bowl-shaped elements and halos had different original compositions, but cannot in isolation distinguish between body and trace fossil explanations for the Khatyspyt material.

From a sedimentological perspective, the most parsimonious explanation for the sedimentological context of the fossil-bearing horizons is that high energy flows created a series of erosive scours, which have first been filled by cross-bedded fine sediment, before being draped by planar laminae (Fig. 2). In individual beds, this is all likely to have happened during one event, with cross-beds preferentially filling the scours as flow velocity decreased, before being draped by planar laminae once the scours were filled. The fossil structures largely lie in and above the planar-laminated part of the beds, although they can also be found (albeit rarely) in the uppermost cross-laminae (e.g. Rogov *et al.* 2012), implying that they were either present and deposited during the later stages of the flow (if they are particles, i.e. body fossils), or were emplaced after sediment deposition had ceased, and cut down through the sedimentary laminae at a later date (if they are trace fossils).

It is possible that the apparent inverse grading results from a progressive increase in the amount of diagenetic overgrowth of silicic material towards the top of the fossil-bearing unit, but it is difficult to determine whether this was the case from the available data (Fig. S2). Assuming that the increased size of elements towards the top of the bed is an original signal, increased nutrient or oxygen availability for trace-making organisms offers a reasonable explanation for the presence of larger burrows closer to the sediment–water interface, in which case the assemblage could be interpreted as a post-turbidite or post-tempestite ichnocoenosis (Leszczyński & Seilacher 1991). However, apparent grading is more readily explained by the sorting of discrete objects in a rapidly deposited sedimentary accumulation.

The observation that the fossil material lies above laminated fine-grained sediment would appear to be at odds with an interpretation of the fossils representing a lag deposit, given that if they were behaving as sedimentary particles settling in a waning flow, they might be expected to exhibit normal grading and to lie at the base of the deposit, following the erosive base as in a traction carpet layer in a granular flow (e.g. Lowe 1982). However, an alternative explanation is that the series and elements behaved as buoyant particles in a clast-rich debris flow. In this scenario, larger clasts would be expected to be entrained towards the top of the flow, resulting in reverse grading of any subsequent deposit. Such an explanation is consistent with the repetition of this sedimentary sequence in the local succession (i.e. successive debrite events), and with the random orientations of individual series in the beds (given that each individual series would have been chaotically transported and then rapidly deposited as flow velocity diminished). Observation of rare isolated elements, both in the Khatyspyt Formation and elsewhere, is explained by the series consisting of transportable objects that could disarticulate into individual elements, and is difficult to explain in a meniscate burrow interpretive framework. A debrite interpretation is also consistent with the general storm- and wave-influenced carbonate ramp depositional environment evidenced by the surrounding beds, and previous interpretation of debris flows in the stratigraphic succession (summarized in the Geological Settings section above). Inverse grading might be expected to involve an upward increase in both clast size and volumetric percentage, which also appears to be the case here (Fig. 1E).

Crucially, if the bed was burrowed or bioturbated, the depth of bioturbation would be expected to be consistent along the length of the bed (i.e. being controlled by the redox gradient in the sediment). Instead, the elements in the Khatyspyt Formation material appear to follow the pre-existing topography of the fine-grained planar laminae at the base of the flow (e.g. Fig. 1C, D). This is inconsistent with expected burrowing behaviour but can be explained by the deposition of particles entrained in a debris flow.

Rogov *et al.* (2012, 2013b) suggested that scouring of the upper surface of the bed, including scours that cut across individual elements in the bed (Fig. 2B), is more compatible with a trace fossil origin for the Khatyspyt material. The observation of scoured elements logically rules out the fossils being originally mineralized (because the scouring currents would not be expected to be strong enough to erode mineralized elements in a soft sediment). Indeed, the occurrence of *Nenoxites* specimens elsewhere as 2D compression fossils (e.g. Kolesnikov *et al.* 2018) provides strong evidence against them having been robustly mineralized original structures. However, an originally soft, sediment filled, or semi-lithified structure could feasibly have been torn or deformed by currents, and there are multiple examples of late Ediacaran organic-walled tubular body fossils that could potentially have behaved in the way we observe if subjected to debris flows. There is uncertainty surrounding both the taphonomic behaviour of invertebrates in debris flows, and the anatomy of these Ediacaran candidate body fossils, but experimental work with modern polychaetes has demonstrated that those soft-bodied organisms can be transported for tens of kilometres in sedimentary density flows without appreciable damage (Bath Enright *et al.* 2017). Assemblages of tubular body fossils from other late Ediacaran deposits (e.g. mineralized *Cloudina* specimens in

the Nama Group of Namibia) can exhibit comparable densities and abundances within individual event beds (Mehra & Maloof 2018), demonstrating that low-diversity accumulations of body fossils are common in comparable late Ediacaran palaeoenvironments. On the balance of available evidence, we consider the sedimentological context of the Khatyspyt Formation *Nenoxites* to be most consistent with a body fossil interpretation for the specimens.

Insights from other global fossil assemblages

Rogov *et al.* (2012) recognized the morphological similarity between Khatyspyt Formation *Nenoxites* material and the late Ediacaran taxa *Shaanxilithes ningqiangensis*, *Helanoichnus helanensis* and *Palaeopascichnus minimus*, *P. meniscatus*, and *P. jiumenensis* from China (e.g. Shen *et al.* 2007; Dong *et al.* 2008; note that the latter taxon, which can be an order of magnitude smaller than the Khatyspyt material, was discussed as a species of *Nenoxites* by Yi *et al.* 2022 and then formally synonymized within *Ordinilunulatus jiumenensis* by Liu *et al.* 2022). Considerable research on those taxa confirms that they reflect body fossils of tubular organisms with an annulated body enclosed in an external tube (Luo & Miao 2020; Wang *et al.* 2021; Liu *et al.* 2022; Yi *et al.* 2022).

Comparisons between *Nenoxites* and tubular body fossils similar to *Shaanxilithes* have precedent (e.g. Hua *et al.* 2004; Shen *et al.* 2007; Cai *et al.* 2011; Meyer *et al.* 2012; Tarhan *et al.* 2014; Ivantsov 2018; Luo & Miao 2020; Wang *et al.* 2021; Yi *et al.* 2022), with some of those authors considering *Nenoxites* to be a tubular body fossil, potentially of protistan grade (Luo & Miao 2020). Such comparisons have been based on both morphological and taphonomic evidence, with some authors noting that multiple taxa may actually reflect taphonomic variants of *Nenoxites curvus* (e.g. Ivantsov 2018). Taxa such as *Helanoichnus*, *Parahorodyskia*, and *Longbizuiella* from the Liuchapo Formation of China (found in association with *Nenoxites* and the morphologically similar taxon *Ordinilunulatus*) can possess similar halos (e.g. Dong *et al.* 2008; Liu *et al.* 2022; Yi *et al.* 2022). Those taxa plus *Shaanxilithes* (note that *Helanoichnus* has been considered a taphonomic variant of *Shaanxilithes ningqiangensis*; Wang *et al.* 2021) possess millimetric internal segments or annulation, sometimes with bridges of material between them (e.g. Luo & Miao 2020; Liu *et al.* 2022; Yi *et al.* 2022). Like *Nenoxites*, *Helanoichnus*, *Longbizuiella* and *Shaanxilithes* can also be preserved either as 2D compressions or 3D silicifications (Chai *et al.* 2021; Yi *et al.* 2022). Some Liuchapo Formation *Nenoxites* taphomorphs show sudden changes in direction (Luo & Miao 2020) and, like the Khatyspyt material, show no evidence for cross-cutting of specimens. *Nenoxites* has been described from strata older than 557.3 ± 0.6 Ma in the Lamtsa Formation of Russia (Grazhdankin 2014; Yang *et al.* 2021) and in the Liuchapo Formation of South China, which lies close to the Ediacaran–Cambrian boundary (540.7 ± 3.8 (±6.6) Ma; Chen & Feng 2019). All globally reported material is of late Ediacaran age and occurs predominantly in silicified deposits, including limestones, siltstones and mudstones (Table 1; Yi *et al.* 2022). This age range corresponds with that of the known range of *Helanoichnus*, *Longbizuiella*, *Ordinilunulatus* and *Shaanxilithes* (Chai *et al.* 2021; Liu *et al.* 2022; Yi *et al.* 2022), while the preservational style hints at a favourable taphonomic window for preservation of such organisms in rock units that have undergone silicification.

Specimens of *Shaanxilithes* from the late Ediacaran of North China have been interpreted as nested internal tubes encased in flexible, annulated external tubes (Wang *et al.* 2021), on the basis of material preserved as compressed 2D structures. Displaced segments in individual series in that material were explained as resulting from compaction or decomposition/partial decay of their surrounding (soft tissue) external tube (Wang *et al.* 2021, fig. 7, red arrows). The 3D material from the Khatyspyt Formation does not show any original cavities inside the elements. However, a gross morphology consisting of a nested, robust internal tube inside a more flexible, potentially unmineralized outer tube (see Wang *et al.* 2021, figs 5–7, 9, 11) could be consistent with the material we describe. In such a scenario, the halo might define the position of the outer tube, while individual elements may reflect the remains of internal body structure. Alternatively, our petrological data indicate that the halos could reflect diagenetic artefacts resulting from the transport of silica to the elements.

The Khatyspyt Formation material can be compared with smaller tubular branching fossils from China showing similar internal segmented 3D morphologies (Sun *et al.* 2019), but the studied material here is non-branching. Yi *et al.* (2022) discussed the similarity of *Nenoxites* and *Palaeopascichnus* specimens from the Liuchapo Formation (see also Luo & Miao 2020), and propose synonymization of *P. minimus*, *P. meniscatus* and *P. jiumensis* within *Nenoxites*. Those authors also erected the new species *Nenoxites irregularis* and *Nenoxites jishouensis* (Yi *et al.* 2022). *Palaeopascichnus jiumenensis* and *N. jishouensis* have since been synonymized in the new taxon *Ordinilunulatus* (Liu *et al.* 2022), which those authors distinguish from *Nenoxites curvus* by their possession of fewer elements, more consistent placement of bridges, and the frequent presence of a terminal spherical structure (Liu *et al.* 2022). However, in all other respects

TABLE 1. Global distribution and stratigraphic occurrence of previously reported *Shaanxilithes/Nenoxites*-like specimens.

Country	Formation	References	Lithology of host unit
China	Zhoujieshan	*Wang *et al.* (1980) Shen *et al.* (2007) (fig. 4:7–8); Wang *et al.* (2021) (figs 3–9) Pang *et al.* (2021) (fig. S3)	Cherts, siltstones and sandstones
	Zhengmuguan	*Yang & Zheng (1985) (pl.1, fig. 8) *Li *et al.* (1997) (pl. 5, fig. 2) Shen *et al.* (2007) (fig. 4: 1–6)	Cherts, siltstones and sandstones
	Yuhucun	*Luo *et al.* (1982) *Luo *et al.* (1988) Luo *et al.* (1991) (no figured specimen) Zhang *et al.* (2015) (figs 3–5) Tang *et al.* (2015) (figs 4–5) Gu *et al.* (2018) (no figured specimen)	Siltstones
	Dengying	*Chen *et al.* (1975) (pl. 1, figs 8–9) *Xing *et al.* (1984) (pl. 8, figs 19–20) *Zhang (1986) (pl. 4, figs 11, 13b) Weber *et al.* (2007) (fig. 6) Cai *et al.* (2011) (fig. 1G–I) Meyer *et al.* (2012) (figs 2, 4) Zhou *et al.* (2019) (fig. 3C) An *et al.* (2020) (fig. 1D–F) Chai *et al.* (2021) (figs 3–4) Fang *et al.* (2021) (figs 4–6)	Limestones, siltstones and mudstones
	Taozichong	Hua *et al.* (2004) (figs 1–6)	Siliceous dolostones at the bottom of Taozichong Formation
	Tuerkeng	Wang *et al.* (2021) (figs 3–9)	Siltstones
	Liuchapo	Dong *et al.* (2008) (figs 7, 10) Wang *et al.* (2012) (fig. 4H) Chen *et al.* (2015) (no figured specimen) Chen & Feng (2019) (fig. 2E–F) Luo & Miao (2020) (figs 3E–G, 4A–K, 6A, 7F–L, 8, 9A–C) Ye *et al.* (2020) (fig. 3A) Yi *et al.* (2022) (figs 3F, 4, 5A–E, 12G–L) Liu *et al.* (2022) (figs 7, 11C–D)	Cherts, siltstones and sandstones
	Laobao	Dong *et al.* (2015) (fig. 3C)	Cherts
	Piyuancun	Dong *et al.* (2012) (fig. 4A–D) Chen & Feng (2019) (no figured specimen)	Siliceous siltstones and shales
Russia	Khatyspyt	Zhuravlev *et al.* (2009) (fig. 2); Rogov *et al.* (2012) (figs 2–3), (2013a) (fig. 1A–B), (2013b) (fig. 1)	Laminated silicified and dolomitized mudstones
	Verkhovka	Fedonkin (1976) Grazhdankin (2014) (fig. 8A–B)	Alternating siltstone and shale, with finely laminated sandstone interbeds
	Yudoma region	Zhuravlev *et al.* (2009) (fig. 2) Ivantsov (2017) (fig. 2D), (2018) (pl. 1, figs 5–7) Wood *et al.* (2017) (fig. 2A)	Calcareous mudstones
Ukraine	Yaryshev	Rogov *et al.* (2013a) (fig. 1C–D)	Tuffaceous silicified mudstones
India	Krol and Tal Groups	Tarhan *et al.* (2014) (fig. 3A–J, 4A–E, H–J)	Siltstones and argillaceous dolostones
Namibia	Nama Group	Darroch *et al.* (2016) (figs 2C–D, 6)	Slabby siltstones and fine-grained sandstones

*Studies that reference material that has not been directly observed by us (either via physical study or observation from photographs).

the morphology of *Ordinilunulatus* is similar to the Khatyspyt material, and ontogenetic or taphonomic factors could be responsible for the stated differences.

Similarly other proposed diagnostic characteristics of those *Nenoxites* species (namely size, mode of preservation, degree of curvature, spacing between elements, and

the irregular nature of element margins) are not considered here to be taxonomically informative; they all have the potential to result from taphonomic processes in the Khatyspyt Formation, and the prevalence of diagenetic silicification and dolomitization at many *Nenoxites* localities worldwide raises concerns that such characters are not original. Given that all variants can commonly be found in the same deposits, we consider it more likely that their different appearance results from taphonomic alteration of a single original morphotype.

There are taxonomic complexities among Ediacaran tubular body fossils that remain to be resolved. The type material of the type species of *Shaanxilithes* (*S. ningqiangensis* Xing *et al.*, 1984) is represented by straight ribbon-like structures *c.* 6–8 mm wide with sharp boundaries and no visible meniscate sub-structure. That type material as originally defined is therefore dissimilar from *Nenoxites curvus*. Conversely, a second species, *Shaanxilithes erodus* Zhang, 1986, does closely resemble *Nenoxites curvus*. There is therefore an argument for synonymization of *Shaanxilithes erodus* with *Nenoxites curvus*, but not the type species *Shaanxilithes ningqiangensis* (and thus the genus *Shaanxilithes*), which seems to represent a distinct taxon. Hua *et al.* (2004) further complicated the issue by expanding the diagnosis of *Shaanxilithes ningqiangensis* and including sinusoidally curved fossils with a meniscate sub-structure that resemble *Nenoxites curvus*. We refrain from formal synonymy at this stage because of the heterogeneous nature of the assemblage currently encompassed by the concept of *Shaanxilithes*, but we note that *Shaanxilithes* as a genus is in need of a thorough revision, and the Khatyspyt *Nenoxites* bear strong similarities to some of the material currently assigned to it. Nevertheless, the Khatyspyt material provides support for the candidacy of the *Shaanxilithes*-type suite of fossils as late Ediacaran (*c.* 558–539 Ma) index fossils (Chai *et al.* 2021; Liu *et al.* 2022).

Affinity

The main challenges to phylogenetic placement of late Ediacaran macrofossils include the uncertainty surrounding the mechanisms by which soft body parts of early animals were preserved, and the difficulty in identifying synapomorphies shared with extant taxa (Cunningham *et al.* 2017). The type species of *Shaanxilithes* (*S. ningqiangensis*) was originally described as a trace fossil (Xing *et al.* 1984), but material assigned to the genus has since been considered as being derived from an alga (Hua *et al.* 2004), a pogonophoran (Chen *et al.* 1975), a foraminifera-like protist (Luo & Miao 2020) or a metazoan of uncertain phylogenetic position (Bengtson & Zhao 1992; Shen *et al.* 2007; Meyer *et al.* 2012; Tarhan *et al.* 2014; Zhang *et al.* 2015). Wang *et al.* (2021) suggested that *Shaanxilithes* is closely related to cloudinids, which are conventionally interpreted as eumetazoans (e.g. Vinn & Zatoń 2012; Schiffbauer *et al.* 2020; Yang *et al.* 2020; Shore & Wood 2021), under the assumption that *Shaanxilithes* has an internal tubular structure composed of nested funnels inside a flexible external sheath. The Khatyspyt *Nenoxites*, and *Shaanxilithes* more generally, may exhibit evidence for histological differentiation into what can be interpreted as distinct tissue layers (Wang *et al.* 2021, fig. 11). Morphologically similar features are achieved by multicellular cyanobacteria, with a mucus sheath enveloping the component cells. However, taphonomy experiments indicate a preservational pathway for multicellular cyanobacteria that contrasts with that seen in *Nenoxites* and *Shaanxilithes*, with the cells degrading rapidly, leaving behind a flaccid sheath (Bartley 1996; Cunningham *et al.* 2012; Manning-Berg *et al.* 2022). Furthermore, the geometry of the compartments and their interconnection is incompatible with a cyanobacterial interpretation. Although eukaryotes are diverse, there are a limited number of multicellular lineages and few of these show histological differentiation. Slime mould fruiting bodies have been interpreted to exhibit epithelia (Dickinson *et al.* 2011, 2012), but their organization is quite distinct from *Nenoxites*. Otherwise, red algae can achieve relatively complex histological differentiation (Dixon 1973; Lobban & Wynne 1981; Cole & Sheath 1990), but there is no evidence that they undergo differential taphonomy (e.g. Xiao *et al.* 2004) and the internal compartments in *Nenoxites* and *Shaanxilithes* are again difficult to rationalize with a rhodophyte interpretation. Furthermore, the red and green algal models are not compatible with evidence that these body fossils comprise a coquina. This leaves metazoans as the only really credible interpretative model. Depending on whether sponges or ctenophores are accepted as the sister-lineage to all other animals (the sponge-sister topology would lead to the inference of epithelial differentiation being a derived trait; e.g. Nielsen 2019), there remains the possibility that *Shaanxilithes* is best interpreted as a total group eumetazoan.

CONCLUSION

Reassessment of fossils from the late Ediacaran Khatyspyt Formation of Siberia suggests that material originally described by Rogov *et al.* (2012) as trace fossils instead reflects a densely packed body fossil coquina of transported, *Shaanxilithes*-like flexible, non-mineralized tubular organisms. Our observations from 3D reconstruction, sedimentology and petrological analysis confirm that the Khatyspyt Formation material is more consistent with a

body fossil origin for *Nenoxites*. The presence of isolated elements; the lack of cross-cutting specimens; the erosive truncation of specimens by beds above; a lack of branching; reverse grading; mineralogically distinct halos; variable shape; sharp directional changes; and the variable presence of bridge structures are all, in combination, more consistent with a body fossil interpretation (Luo & Miao 2020; Liu *et al.* 2022; Yi *et al.* 2022). These observations supplement previously made arguments against an ichnological origin for Khatyspyt *Nenoxites* (Brasier *et al.* 2013; Gámez Vintaned & Zhuravlev 2013) including the presence of connections between the proposed 'menisci' and the inconsistent morphology and size of the elements, and emphasize the similarity of *Nenoxites* material to *Shaanxilithes*-type body fossil material from South China. The taxonomy of such specimens is in need of considerable revision in light of these and other recent discussions (e.g. Luo & Miao 2020; Chai *et al.* 2021; Wang *et al.* 2021; Liu *et al.* 2022; Yi *et al.* 2022).

The body fossil interpretation of Khatyspyt *Nenoxites* shifts the origin of sediment-penetrative burrowing and bioturbation (most probably indicative of bilaterian animals) closer to the Ediacaran–Cambrian boundary. The current oldest examples of sediment-penetrative burrows and patches of bioturbation now occur in offshore marine environments in the latest Ediacaran Period (e.g. Mángano & Buatois 2020; Darroch *et al.* 2021), with bioturbation not reaching substantial intensities until Cambrian Age 2 (Mángano & Buatois 2020). Our results also expand the range of taphonomic variability exhibited by tubular organisms that are candidates for latest Ediacaran index fossils. Finally, *Shaanxilithes*-type body fossils are likely to reflect an addition to the diversity of candidate metazoans in the late Ediacaran.

Acknowledgements. We thank B. Buse, T. Davies and S. Kearns for technical support, M. Tucker for discussion, and S. Jensen, R. Wood and A. Penny for providing *Cloudina* specimens for comparative analysis. We appreciate the assistance of Z. Chen for translating sections of Chinese-language publications. Stratigraphic, sedimentological and palaeoecological studies of the Khatyspyt Formation were supported by the Russian Science Foundation (grant 20-67-46028 to DVG). We thank the two anonymous reviewers and James D. Schiffbauer for greatly improving the text. Analyses were conducted by CP in partial fulfilment of the MSc Palaeobiology at the University of Bristol, and supported by NERC (NE/L011409/1 to AGL and NE/P013678/1 to AGL and PCJD, part of the Biosphere Evolution, Transitions and Resilience (BETR) programme, co-funded by the Natural Science Foundation of China (NSFC)). PCJD was also funded by a Leverhulme Trust Research Fellowship (RF-2022-167). LAP was supported by an early career fellowship from St Edmund Hall, Oxford and a NERC Independent Research Fellowship (grant no. NE/W007878/1). DVG and VIR were supported by Government Contract FWZZ-2022-0002 (Fundamental Scientific Research Programme of the Russian Federation).

Author contributions. **Conceptualization** AG Liu (AGL); **Data Curation** PCJ Donoghue (PCJD), RJ Garwood (RJG), LA Parry (LAP), AGL; **Formal Analysis** Christos Psarras (CP), PCJD, AGL; **Funding Acquisition** AGL; **Investigation** CP, DV Grazhdankin (DVG); **Methodology** CP; **Project Administration** CP, AGL; **Resources** DVG, VI Rogov (VIR), AGL; **Software** CP, RJG, LAP; **Supervision** PCJD, DVG, AGL; **Validation** CP; **Visualization** CP, RJG, LAP, AGL; **Writing – Original Draft Preparation** CP; **Writing – Review & Editing** CP, PCJD, RJG, DVG, LAP, VIR, AGL.

DATA ARCHIVING STATEMENT

Data for this study (including the CT datasets and a 3D model) are available in the Bristol Data Repository: https://doi.org/10.5523/bris.13jspoe3ih1wl2bx94tc6x6uf7

Editor. Imran Rahman

SUPPORTING INFORMATION

Additional Supporting Information can be found online (https://doi.org/10.1002/spp2.1531):

Figure S1. SEM elemental maps and spectrum showing the margin of an element and the surrounding sedimentary matrix.
Figure S2. Annotated photomosaic in plane polarized transmitted light showing thin section CAMSM X 50382.2.1, and the variation in appearance and mineralogy of the Khatyspyt *Nenoxites* fossil material through the studied bed.

REFERENCES

AN, Z.-H., ZHAO, X.-M., NIU, Z.-J., LI, Z.-H. and YE, Q. 2020. Discovery of *Shaanxilithes* from the Dengying Formation in the Yangtze Gorges area, South China, and its stratigraphic significance. *China Geology*, **3**, 649–651.

BARTLEY, J. K. 1996. Actualistic taphonomy of cyanobacteria: implications for the Precambrian fossil record. *PALAIOS*, **11**, 571–586.

BATH ENRIGHT, O. G., MINTER, N. J. and SUMNER, E. J. 2017. Palaeoecological implications of the preservation potential of soft-bodied organisms in sediment-density flows: testing turbulent waters. *Royal Society Open Science*, **4**, 170212.

BENGTSON, S. and ZHAO, Y. 1992. Predatorial borings in Late Precambrian mineralized exoskeletons. *Science*, **257**, 367–369.

BLINKENBERG, K. H., ANDERSKOUV, K., SØLLING, T. I., AL-RAMADAN, K. and STEMMERIK, L. 2021. The influence of silica on carbonate diagenesis in chalk: Ekofisk Formation, Danish Central Graben. *Sedimentary Geology*, **415**, 105846.

BOTTJER, D. J., HAGADORN, J. W. and DORNBOS, S. Q. 2000. The Cambrian substrate revolution. *GSA Today*, **10** (9), 1–7.

BOWRING, S. A., GROTZINGER, J. P., ISACHSEN, C. E., KNOLL, A. H., PELECHATY, S. M. and KOLOSOV, P. 1993. Calibrating rates of Early Cambrian evolution. *Science*, **261**, 1293–1298.

BRASIER, M. D., COWIE, J. and TAYLOR, M. 1994. Decision on the Precambrian–Cambrian boundary. *Episodes*, **17**, 95–100.

BRASIER, M. D., McILROY, D., LIU, A. G., ANTCLIFFE, J. B. and MENON, L. R. 2013. The oldest evidence of bioturbation on Earth: Comment. *Geology*, **41**, e289.

BUATOIS, L. A. and MÁNGANO, M. G. 2011. *Ichnology: Organism–substrate interactions in space and time*. Cambridge University Press, 366 pp.

BUATOIS, L. A. and MÁNGANO, M. G. 2016. Ediacaran ecosystems and the dawn of animals. 27–72. *In* MÁNGANO, M. and BUATOIS, L. (eds) *The trace-fossil record of major evolutionary events*. Springer. Topics in Geobiology, **39**.

BUDD, G. E. and JENSEN, S. 2000. A critical reappraisal of the fossil record of the bilaterian phyla. *Biological Reviews*, **75**, 253–295.

BUTTS, S. H. 2014. Silicification. *The Paleontological Society Papers*, **20**, 15–34.

BYKOVA, N., GILL, B. C., GRAZHDANKIN, D., ROGOV, V. and XIAO, S. 2017. A geochemical study of the Ediacaran discoidal fossil *Aspidella* preserved in limestones: implications for its taphonomy and paleoecology. *Geobiology*, **15**, 572–587.

BYKOVA, N., LODUCA, S. T., YE, Q., MARUSIN, V., GRAZHDANKIN, D. and XIAO, S. 2020. Seaweeds through time: morphological and ecological analysis of Proterozoic and early Palaeozoic benthic macroalgae. *Precambrian Research*, **350**, 105875.

CAI, Y., HUA, H., ZHURAVLEV, A. Yu., GÁMEZ VINTANED, J. and IVANTSOV, A. 2011. Discussion of 'First finds of problematic Ediacaran fossil *Gaojiashania* in Siberia and its origin'. *Geological Magazine*, **148**, 329–333.

CAI, Y., XIAO, S., LI, G. and HUA, H. 2019. Diverse biomineralizing animals in the terminal Ediacaran Period herald the Cambrian explosion. *Geology*, **47**, 380–384.

CARBONE, C. and NARBONNE, G. M. 2014. When life got smart: the evolution of behavioral complexity through the Ediacaran and early Cambrian of NW Canada. *Journal of Paleontology*, **88**, 309–330.

CHAI, S., WU, Y. and HUA, H. 2021. Potential index fossils for the Terminal Stage of the Ediacaran System. *Journal of Asian Earth Sciences*, **218**, 104885.

CHEN, C. and FENG, Q. 2019. Carbonate carbon isotope chemostratigraphy and U-Pb zircon geochronology of the Liuchapo Formation in South China: constraints on the Ediacaran–Cambrian boundary in deep-water sequences. *Palaeogeography, Palaeoclimatology, Palaeoecology*, **535**, 109361.

CHEN, M. E., CHEN, X. G. and LAO, Q. Y. 1975. An introduction to the Metazoa fossil from the upper Sinian System in southern Shensi and its stratigraphic significance. *Scientia Geologica Sinica*, **2**, 181–192. [in Chinese with English abstract]

CHEN, D., ZHOU, X., FU, Y., WANG, J. and YAN, D. 2015. New U–Pb zircon ages of the Ediacaran–Cambrian boundary strata in South China. *Terra Nova*, **27**, 62–68.

CHEN, Z., CHEN, X., ZHOU, C., YUAN, X. and XIAO, S. 2018. Late Ediacaran trackways produced by bilaterian animals with paired appendages. *Science Advances*, **4** (6), eaao6691.

CHEN, Z., ZHOU, C., YUAN, X. and XIAO, S. 2019. Death march of a segmented and trilobate bilaterian elucidates early animal evolution. *Nature*, **573**, 412–415.

CHERRY, L. B., GILLEAUDEAU, G. J., GRAZHDANKIN, D. V., ROMANIELLO, S. J., MARTIN, A. J. and KAUFMAN, A. J. 2022. A diverse Ediacara assemblage survived under low-oxygen conditions. *Nature Communications*, **13**, 7306.

COLE, K. M. and SHEATH, R. G. 1990. *Biology of the red algae*. Cambridge University Press.

CUNNINGHAM, J. A., THOMAS, C.-W., BENGTSON, S., MARONE, F., STAMPANONI, M., TURNER, F. R., BAILEY, J. V., RAFF, R. A., RAFF, E. C. and DONOGHUE, P. C. J. 2012. Experimental taphonomy of giant sulphur bacteria: implications for the interpretation of the embryo-like Ediacaran Doushantuo fossils. *Proceedings of the Royal Society B*, **279**, 1857–1864.

CUNNINGHAM, J. A., LIU, A. G., BENGTSON, S. and DONOGHUE, P. C. J. 2017. The origin of animals: can molecular clocks and the fossil record be reconciled? *BioEssays*, **39**, e201600120.

DARROCH, S. A. F., BOAG, T. H. and RACICOT, R. A. 2016. A mixed Ediacaran-metazoan assemblage from the Zaris Sub-basin, Namibia. *Palaeogeography, Palaeoclimatology, Palaeoecology*, **459**, 198–208.

DARROCH, S. A. F., CRIBB, A. T., BUATOIS, L. A., GERMS, G. J. B., KENCHINGTON, C. G., SMITH, E. F., MOCKE, H., O'NEIL, G. R., SCHIFFBAUER, J. D., MALONEY, K. M., RACICOT, R. A., TURK, K. A., GIBSON, B. M., ALMOND, J., KOESTER, B., BOAG, T. H., TWEEDT, S. M. and LAFLAMME, M. 2021. The trace fossil record of the Nama Group, Namibia: exploring the terminal Ediacaran roots of the Cambrian explosion. *Earth-Science Reviews*, **212**, 103435.

DICKINSON, D. J., NELSON, W. J. and WEIS, W. I. 2011. A polarised epithelium organised by beta and alpha catenin predates cadherin and metazoan origins. *Science*, **331**, 1336–1339.

DICKINSON, D. J., NELSON, W. J. and WEIS, W. I. 2012. An epithelial tissue in *Dictyostelium* challenges the traditional origin of metazoan multicellularity. *BioEssays*, **34**, 833–840.

DIXON, P. S. 1973. *Biology of the Rhodophyta*. Oliver and Boyd.

DONG, L., XIAO, S., SHEN, B. and ZHOU, C. 2008. Silicified *Horodyskia* and *Palaeopaschichnus* from upper Ediacaran cherts in South China: tentative phylogenetic interpretation and implications for evolutionary stasis. *Journal of the Geological Society*, **165**, 367–378.

DONG, L., SONG, W., XIAO, S., YUAN, X., CHEN, Z. and ZHOU, C. 2012. Micro- and macrofossils from the Piyuancun Formation and their implications for the Ediacaran–Cambrian boundary in southern Anhui. *Journal of Stratigraphy*, **36**, 600–610.

DONG, L., SHEN, B., LEE, C.-T. A., SHU, X., PENG, Y., SUN, Y., TANG, Z., RONG, H., LANG, X., MA, H., YANG, F. and GUO, W. 2015. Germanium/silicon of the Ediacaran–Cambrian Laobao cherts: implications for the bedded chert formation and paleoenvironment interpretations. *Geochemistry, Geophysics, Geosystems*, **16**, 751–763.

dos REIS, M., THAWORNWATTANA, Y., ANGELIS, K., TELFORD, M. J., DONOGHUE, P. C. J. and YANG, Z. 2015. Uncertainty in the timing of origin of animals and the limits of precision in molecular timescales. *Current Biology*, **25**, 2939–2950.

DUDA, J.-P., THIEL, V., REITNER, J. and GRAZHDANKIN, D. 2016. Opening up a window into ecosystems with Ediacara-type organisms: preservation of molecular fossils in the Khatyspyt Lagerstätte (Arctic Siberia). *PalZ*, **90**, 659–671.

DUDA, J.-P., LOVE, G. D., ROGOV, V. I., MELNIK, D. S., BLUMENBERG, M. and GRAZHDANKIN, D. V. 2020. Understanding the geobiology of the terminal Ediacaran Khatyspyt Lagerstätte (Arctic Siberia, Russia). *Geobiology*, **18**, 643–662.

DUNN, F. S., LIU, A. G. and GEHLING, J. G. 2019. Anatomical and ontogenetic reassessment of the Ediacaran frond *Arborea arborea* and its placement within total group Eumetazoa. *Palaeontology*, **62**, 851–865.

DUNN, F. S., LIU, A. G., GRAZHDANKIN, D., VIXSEBOXSE, P., FLANNERY-SUTHERLAND, J., GREEN, E., HARRIS, S. and DONOGHUE, P. C. J. 2021. The developmental biology of *Charnia* and the eumetazoan affinity of the Ediacaran rangeomorphs. *Science Advances*, **7** (30), eabe0291.

DUNN, F. S., KENCHINGTON, C. G., PARRY, L. A., CLARK, J. W., KENDAL, R. S. and WILBY, P. R. 2022. A crown-group cnidarian from the Ediacaran of Charnwood Forest, UK. *Nature Ecology & Evolution*, **6**, 1095–1104.

ERWIN, D. H., LAFLAMME, M., TWEEDT, S. M., SPERLING, E. A., PISANI, D. and PETERSON, K. J. 2011. The Cambrian conundrum: early divergence and later ecological success in the early history of animals. *Science*, **334**, 1091–1097.

EVANS, S. D., DROSER, M. L. and GEHLING, J. G. 2017. Highly regulated growth and development of the Ediacara macrofossil *Dickinsonia costata*. *PLoS One*, **12**, e0176874.

EVANS, S. D., HUGHES, I. V., GEHLING, J. G. and DROSER, M. L. 2020. Discovery of the oldest bilaterian from the Ediacaran of South Australia. *Proceedings of the National Academy of Sciences*, **117**, 7845–7850.

FANG, R., LIANG, Y., HUA, H. and ZHANG, Z. 2021. First report of the problematic Ediacaran fossil *Shaanxilithes* from the Jiu-cheng Member of Zhujiaqing Section in Huize, Yunnan Province. *Acta Palaeontologica Sinica*, **60** (1), 2020035.

FEDONKIN, M. A. 1976. Traces of multicellular animals in the Valdai Group. *Izvestiya Akademii Nauk SSSR, Seriya Geologicheskaya*, **4**, 129–132.

FEDONKIN, M. A. 1988. Paleoichnology of the Precambrian–Cambrian transition in the Russian Platform and Siberia. 12. *In* LANDING, E., NARBONNE, G. M. and MYROW, P. (eds) *Trace fossils, small shelly fossils and the Precambrian–Cambrian boundary*. New York State Museum, Bulletin, **463**.

FEDONKIN, M. A. 1990. Systematic description of Vendian metazoa. 71–120. *In* SOKOLOV, B. S. and IVANOVSKIJ, A. B. (eds) *The Vendian system. Vol. 1 Paleontology*. Springer.

FEDONKIN, M. A. and WAGGONER, B. M. 1997. The Late Precambrian fossil *Kimberella* is a mollusc-like bilaterian organism. *Nature*, **388**, 868–871.

GÁMEZ VINTANED, J. A. and ZHURAVLEV, A. Yu. 2013. The oldest evidence of bioturbation on Earth: Comment. *Geology*, **41**, e299.

GARWOOD, R. and DUNLOP, J. 2014. The walking dead: blender as a tool for paleontologists with a case study on extinct arachnids. *Journal of Paleontology*, **88**, 735–746.

GEHLING, J. G. and DROSER, M. L. 2018. Ediacaran scavenging as a prelude to predation. *Emerging Topics in Life Sciences*, **2**, 213–222.

GOLD, D. A., RUNNEGAR, B., GEHLING, J. G. and JACOBS, D. K. 2015. Ancestral state reconstruction of ontogeny supports a bilaterian affinity for *Dickinsonia*. *Evolution & Development*, **17**, 315–324.

GRAZHDANKIN, D. 2014. Patterns of evolution of the Ediacaran soft-bodied biota. *Journal of Paleontology*, **88**, 269–283.

GRAZHDANKIN, D., BALTHASAR, U., NAGOVITSIN, K. E. and KOCHNEV, B. B. 2008. Carbonate-hosted Avalon-type fossils in arctic Siberia. *Geology*, **36**, 803–806.

GU, P., ZHONG, L., ZHANG, G. D., SONG, S. C., TANG, F., LING, M. Q. and GAO, L. Z. 2018. The division of the Late Ediacaran–Cambrian boundary interval stratigraphy and new options of index fossil FAD in south China. *Acta Geologica Sinica*, **3**, 449–465.

HUA, H., CHEN, Z. and ZHANG, L. 2004. *Shaanxilithes* from Taozichong Formation of Guizhou Province and its significance. *Journal of Stratigraphy*, **28**, 265–269. [in Chinese with English abstract]

IVANTSOV, A. Y. 2017. Finds of Ediacaran-type fossils in Vendian deposits of the Yudoma Group, Eastern Siberia. *Doklady Earth Sciences*, **472**, 143–146.

IVANTSOV, A. Y. 2018. Vendian macrofossils of the Yudoma Group, southeast of the Siberian platform. *Paleontological Journal*, **52**, 1335–1346.

KNOLL, A. H., GROTZINGER, J. P., KAUFMAN, A. J. and KOLOSOV, P. 1995. Integrated approaches to terminal Proterozoic stratigraphy: an example from the Olenek Uplift, northeastern Siberia. *Precambrian Research*, **73**, 251–270.

KOLESNIKOV, A. V., ROGOV, V. I., BYKOVA, N., TANELIAN, D., CLAUSEN, S., MASLOV, A. V. and GRAZHDANKIN, D. V. 2018. The oldest skeletal macroscopic organism *Palaeopascichnus linearis*. *Precambrian Research*, **316**, 24–37.

LESZCZYŃSKI, S. and SEILACHER, A. 1991. Ichnocoenoses of a turbidite sole. *Ichnos*, **1**, 293–303.

LI, R. H., YANG, S. P. and LI, W. Q. 1997. *Trace fossils from Sinian–Cambrian boundary strata in China*. Geological Publishing House, Beijing, 99 pp. [in Chinese with English Abstract]

LIMAYE, A. 2012. Drishti: a volume exploration and presentation tool. *Proceedings SPIE 8506, Developments in X-ray Tomography VIII*, **85060x**, 191–199.

LIU, A. G., McILROY, D. and BRASIER, M. D. 2010. First evidence for locomotion in the Ediacara biota from the 565 Ma Mistaken Point Formation, Newfoundland. *Geology*, **38**, 123–126.

LIU, A. G., MATTHEWS, J. J., MENON, L. R., McILROY, D. and BRASIER, M. D. 2014. *Haootia quadriformis* n. gen., n. sp., interpreted as a muscular cnidarian impression from the Late Ediacaran period (approx. 560 Ma). *Proceedings of the Royal Society B*, **281**, 20141202.

LIU, H., DONG, L., QIN, S., LIU, W. and LI, C. 2022. Restudy of string fossils from the Ediacaran–Cambrian Liuchapo Formation in Guizhou Province, South China. *Precambrian Research*, **376**, 106693.

LOBBAN, C. S. and WYNNE, M. J. 1981. *The biology of seaweeds*. University of California Press.

LOWE, D. R. 1982. Sediment gravity flows; II, depositional models with special reference to the deposits of high-density turbidity currents. *Journal of Sedimentary Research*, **52**, 279–297.

LUO, C. and MIAO, L. Y. 2020. A *Horodyskia–Nenoxites*-dominated fossil assemblage from the Ediacaran–Cambrian transition (Liuchapo Formation, Hunan Province): its paleontological implications and stratigraphic potential. *Palaeogeography, Palaeoclimatology, Palaeoecology*, **545**, 109635.

LUO, H. L., JIANG, Z. W., WU, X. C. and SONG, X. L. 1982. *Sinian–Cambrian boundary of Eastern Yunnan*. Yunnan People's Publishing House, Kunming, 72 pp.

LUO, H. L., WU, X. C., OUYANG, L., JIANG, Z. W. and SONG, X. L. 1988. New correlation opinions on the sections of Sinian–Cambrian boundary in the Yangtze Platform. *Yunnan Geology*, **7**, 13–27.

LUO, H., WU, X. and OUYANG, L. 1991. Facies changes and transverse correlation of the Sinian–Cambrian boundary strata in Eastern Yunnan. *Sedimentary Geology & Tethyan Geology*, **11** (4), 27–35.

MACDONALD, F. A., PRUSS, S. B. and STRAUSS, J. V. 2014. Trace fossils with spreiten from the Late Ediacaran Nama Group, Namibia: complex feeding patterns five million years before the Precambrian–Cambrian boundary. *Journal of Paleontology*, **88**, 299–308.

MÁNGANO, M. G. and BUATOIS, L. A. 2014. Decoupling of body-plan diversification and ecological structuring during the Ediacaran–Cambrian transition: evolutionary and geobiological feedbacks. *Proceedings of the Royal Society B*, **281** (1780), 20140038.

MÁNGANO, M. G. and BUATOIS, L. A. 2017. The Cambrian revolutions: trace-fossil record, timing, links and geobiological impact. *Earth-Science Reviews*, **173**, 96–108.

MÁNGANO, M. G. and BUATOIS, L. A. 2020. The rise and early evolution of animals: where do we stand from a trace-fossil perspective? *Interface Focus*, **10**, 20190103.

MANNING-BERG, A., SELLY, T. and BARTLEY, J. K. 2022. Actualistic approaches to interpreting the role of biological decomposition in microbial preservation. *Geobiology*, **20**, 216–232.

MATTHEWS, J. J., LIU, A. G., YANG, C., McILROY, D., LEVELL, B. and CONDON, D. J. 2021. A chronostratigraphic framework for the rise of the Ediacaran macrobiota: new constraints from Mistaken Point Ecological Reserve, Newfoundland. *GSA Bulletin*, **133**, 612–624.

McILROY, D. and LOGAN, G. A. 1999. The impact of bioturbation on infaunal ecology and evolution during the Proterozoic–Cambrian transition. *PALAIOS*, **14**, 58–72.

MENON, L. R., McILROY, D. and BRASIER, M. D. 2013. Evidence for Cnidaria-like behavior in ca. 560 Ma Ediacaran *Aspidella*. *Geology*, **41**, 895–898.

MEHRA, A. and MALOOF, A. 2018. Multiscale approach reveals that *Cloudina* aggregates are detritus and not in situ reef constructions. *Proceedings of the National Academy of Sciences*, **115**, E2519–E2527.

MEYER, M., SCHIFFBAUER, J. D., XIAO, S., CAI, Y. and HUA, H. 2012. Taphonomy of the upper Ediacaran enigmatic ribbon-like fossil *Shaanxilithes*. *PALAIOS*, **27**, 354–372.

MEYER, M., XIAO, S., GILL, B. C., SCHIFFBAUER, J. D., CHEN, Z., ZHOU, C. and YUAN, X. 2014. Interactions between Ediacaran animals and microbial mats: insights from *Lamonte trevallis*, a new trace fossil from the Dengying Formation of South China. *Palaeogeography, Palaeoclimatology, Palaeoecology*, **396**, 62–74.

NAGOVITSIN, K. E., ROGOV, V. I., MARUSIN, V. V., KARLOVA, G. A., KOLESNIKOV, A. V., BYKOVA, N. V. and GRAZHDANKIN, D. V. 2015. Revised Neoproterozoic and Terreneuvian stratigraphy of the Lena-Anabar Basin and north-western slope of the Olenek Uplift, Siberian Platform. *Precambrian Research*, **270**, 226–245.

NIELSEN, C. 2019. Early animal evolution: a morphologist's view. *Royal Society Open Science*, **6** (7), 190638.

PANG, K., WU, C., SUN, Y., OUYANG, Q., YUAN, X., SHEN, B., LANG, X., WANG, R., CHEN, Z. and ZHOU, C. 2021. New Ediacara-type fossils and late Ediacaran stratigraphy from the northern Qaidam Basin (China): paleogeographic implications. *Geology*, **49**, 1160–1164.

PARRY, L. A., BOGGIANI, P. C., CONDON, D. J., GARWOOD, R. J., LEME, J. M., McILROY, D., BRASIER, M. D., TRINDADE, R., CAMPANHA, G. A. C., PACHECO, M. L. A. F., DINIZ, C. Q. C. and LIU, A. G. 2017. Ichnological evidence for meiofaunal bilaterians from the terminal Ediacaran and earliest Cambrian of Brazil. *Nature Ecology & Evolution*, **1**, 1455–1464.

PELECHATY, S. M., KAUFMAN, A. J. and GROTZINGER, J. P. 1996. Evaluation of $\delta^{13}C$ chemostratigraphy for intrabasinal correlation: Vendian strata of northeast Siberia. *Geological Society of America Bulletin*, **108**, 992–1003.

PSARRAS, C., DONOGHUE, P. C. J., GARWOOD, R. J., GRAZHDANKIN, D. V., PARRY, L. A., ROGOV, V. I. and LIU, A. G. 2023. Data from Psarras et al. 2023. Three-dimensional reconstruction, taphonomic and petrological data suggest the oldest record of bioturbation is a body fossil coquina. Papers in Palaeontology. Bristol Data Repository. https://doi.org/10.5523/bris.13jspoe3ih1wl2bx94tc6x6uf7

ROGOV, V. I., MARUSIN, V., BYKOVA, N., GOY, Y., NAGOVITSIN, K. E., KOCHNEV, B. B., KARLOVA, G. A. and GRAZHDANKIN, D. 2012. The oldest evidence of bioturbation on Earth. *Geology*, **40**, 395–398.

ROGOV, V. I., MARUSIN, V., BYKOVA, N., GOY, Y., NAGOVITSIN, K. E., KOCHNEV, B. B., KARLOVA, G. A. and GRAZHDANKIN, D. 2013a. The oldest evidence of bioturbation on Earth: Reply. *Geology*, **41** (5), e290.

ROGOV, V. I., MARUSIN, V., BYKOVA, N., GOY, Y., NAGOVITSIN, K. E., KOCHNEV, B. B., KARLOVA, G. A. and GRAZHDANKIN, D. 2013b. The oldest evidence of bioturbation on Earth: Reply. *Geology*, **41** (9), e300.

SCHIFFBAUER, J. D., SELLY, T., JACQUET, S. M., MERZ, R. A., NELSON, L. L., STRANGE, M. A., CAI, Y. and SMITH, E. F. 2020. Discovery of bilaterian-type through-guts in cloudinomorphs from the terminal Ediacaran Period. *Nature Communications*, **11** (1), 205.

SEILACHER, A. 1989. Vendozoa: organismic construction in the Proterozoic biosphere. *Lethaia*, **22**, 229–239.

SHEN, B., XIAO, S., DONG, L., ZHOU, C. and LIU, J. 2007. Problematic macrofossils from Ediacaran successions in the North China and Chaidam blocks: implications for their evolutionary roots and biostratigraphic significance. *Journal of Paleontology*, **81**, 1396–1411.

SHORE, A. and WOOD, R. 2021. Environmental and diagenetic controls on the morphology and calcification of the Ediacaran metazoan *Cloudina*. *Scientific Reports*, **11** (1), 12341.

SOKOLOV, B. S. and FEDONKIN, M. A. 1984. The Vendian as the terminal system of the Precambrian. *Episodes*, **7**, 12–19.

SUN, W.-C., YIN, Z.-J., DONOGHUE, P. C. J., LIU, P.-J., SHANG, X.-D. and ZHU, M.-Y. 2019. Tubular microfossils from the Ediacaran Weng'an Biota (Doushantuo Formation, South China) are not early animals. *Palaeoworld*, **28**, 469–477.

SUTTON, M. D., GARWOOD, R. J., SIVETER, D. J. and SIVETER, D. J. 2012. SPIERS and VAXML; a software toolkit for tomographic visualisation and a format for virtual specimen interchange. *Palaeontologia Electronica*, **15** (2), 5T.

TANG, F., GAO, L. Z., YIN, C. Y., WANG, Y. and GU, P. 2015. Macrofossil biotas in the Late Ediacaran–Cambrian boundary interval of South China and stratotype correlation. *Geological Bulletin of China*, **34**, 2150–2162.

TARHAN, L. G. 2018. The early Paleozoic development of bioturbation: evolutionary and geobiological consequences. *Earth-Science Reviews*, **178**, 177–207.

TARHAN, L. G., HUGHES, N. C., MYROW, P. M., BHARGAVA, O. N., AHLUWALIA, A. D. and KUDRYAVTSEV, A. B. 2014. Precambrian–Cambrian boundary interval occurrence and form of the enigmatic tubular body fossil *Shaanxilithes ningqiangensis* from the Lesser Himalaya of India. *Palaeontology*, **57**, 283–298.

TARHAN, L. G., MYROW, P. M., SMITH, E. F., NELSON, L. L. and SADLER, P. M. 2020. Infaunal augurs of the Cambrian explosion: an Ediacaran trace fossil assemblage from Nevada, USA. *Geobiology*, **18**, 486–496.

TURK, K. A., MALONEY, K. M., LAFLAMME, M. and DARROCH, S. A. F. 2022. Paleontology and ichnology of the late Ediacaran Nasep–Huns transition (Nama Group, southern Namibia). *Journal of Paleontology*, **96**, 753–769.

VINN, O. and ZATOŃ, M. 2012. Inconsistencies in proposed annelid affinities of early biomineralized organism *Cloudina* (Ediacaran): structural and ontogenetic evidences. *Carnets de Géologie*, **2012/03** (CG2012_A03), 39–47.

VODANJUK, S. A. 1989. Non-skeletal fossil Metazoa from the Khatyspyt formation of the Olenek Uplift. 61–74. *In* KHOMENTOVSKY, V. V. and SOVETOV, J. K. (eds) *Late Precambrian and Early Palaeozoic of Siberia: Urgent stratigraphic problems*. Institute of Geology & Geophysics, Novosibirsk. [in Russian]

WANG, Y., ZHUANG, Q., SHI, C., LIU, J. and ZHENG, L. 1980. Quanji group along the northern border of Chaidamu Basin. 214–229. *In* TIANJIN INSTITUTE OF GEOLOGY AND MINERAL RESOURCES (ed.) *Research on Precambrian Geology, Sinian Suberathem in China*. Tianjing Science and Technology Press. [in Chinese without English abstract]

WANG, J. G., CHEN, D. Z., WAN, D., YAN, D. T. and ZHOU, X. Q. 2012. Petrology and geochemistry of chert on the marginal zone of Yangtze Platform, western Hunan, South China, during the Ediacaran–Cambrian transition. *Sedimentology*, **59**, 809–829.

WANG, X., ZHANG, X., ZHANG, Y., CUI, L. and LI, L. 2021. New materials reveal *Shaanxilithes* as a *Cloudina*-like organism of the late Ediacaran. *Precambrian Research*, **362**, 106277.

WEBER, B., STEINER, M. and ZHU, M.-Y. 2007. Precambrian–Cambrian trace fossils from the Yangtze Platform (South China) and the early evolution of bilaterian lifestyles. *Palaeogeography, Palaeoclimatology, Palaeoecology*, **254**, 328–349.

WILLMAN, S. and SLATER, B. J. 2021. Late Ediacaran organic microfossils from Finland. *Geological Magazine*, **158**, 2231–2244.

WOOD, R. A., ZHURAVLEV, A. Yu., SUKHOV, S. S., ZHU, M. and ZHAO, F. 2017. Demise of Ediacaran dolomitic seas marks widespread biomineralization on the Siberian Platform. *Geology*, **45**, 27–30.

XIAO, S., KNOLL, A. H., YUAN, X. and PUESCHEL, C. M. 2004. Phosphatized multicellular algae in the Neoproterozoic Doushantuo Formation, China, and the early evolution of florideophyte red algae. *American Journal of Botany*, **91**, 214–227.

XIAO, S., CHEN, Z., ZHOU, C. and YUAN, X. 2019. Surfing in and on microbial mats: oxygen-related behavior of a terminal Ediacaran bilaterian animal. *Geology*, **47**, 1054–1058.

XING, Y., DING, Q., LUO, H., HE, T. and WANG, Y. 1984. The Sinian–Cambrian boundary of China. *Bulletin of the Institute of Geology, Chinese Academy of Geological Sciences*, **10**, 1–262. [in Chinese with English abstract]

YANG, S. P. and ZHENG, Z. C. 1985. The Sinian trace fossils from Zhengmuguan Formation of Helanshan Mountain, Ningxia. *Earth Science: Journal of Wuhan College of Geology*, **10**, 9–18.

YANG, B., STEINER, M., SCHIFFBAUER, J. D., SELLY, T., WU, X., ZHANG, C. and LIU, P. 2020. Ultrastructure of Ediacaran cloudinids suggests diverse taphonomic histories and affinities with non-biomineralized annelids. *Scientific Reports*, **10** (1), 535.

YANG, C., ROONEY, A. D., CONDON, D. J., LI, X.-H., GRAZHDANKIN, D. V., BOWYER, F. T., HU, C., MACDONALD, F. A. and ZHU, M. 2021. The tempo of Ediacaran evolution. *Science Advances*, **7**, eabi9643.

YE, Y., SHEN, J., FENG, Q. and LASH, G. G. 2020. Microbial and animal evolution in relation to redox fluctuations in a deep-water setting of South China during the Ediacaran–Cambrian transition (ca. 551–523 Ma). *Palaeogeography, Palaeoclimatology, Palaeoecology*, **546**, 109672.

YI, Y., CHEN, F., ALGEO, T. J. and FENG, Q. 2022. Deep-water fossil assemblages from the Ediacaran–Cambrian transition of western Hunan, South China and their biostratigraphic and evolutionary implications. *Palaeogeography, Palaeoclimatology, Palaeoecology*, **591**, 110878.

ZHANG, L. Y. 1986. A discovery and preliminary study of the late stage of late Gaojiashan Biota from Sinian in Ningqiang County, Shaanxi. *Bulletin of the Xi'an Institute of Geology and Mineral resources, Chinese Academy of Geological Sciences*, **13**, 67–88. [in Chinese with English Abstract]

ZHANG, Z. L., HUA, F. and ZHANG, Z. F. 2015. Problematic Ediacaran fossil *Shaanxilithes* from the Jiucheng Member of Wangjiawan section in Jinning, Yunnan Province. *Acta Palaeontologica Sinica*, **54**, 12–28.

ZHOU, C., YUAN, X., XIAO, S., CHEN, Z. and HUA, H. 2019. Ediacaran integrative stratigraphy and timescale of China. *Science China Earth Sciences*, **62**, 7–724.

ZHU, M., ZHURAVLEV, A. Yu., WOOD, R. A., ZHAO, F. and SUKHOV, S. S. 2017. A deep root for the Cambrian explosion: implications of new bio- and chemostratigraphy from the Siberian Platform. *Geology*, **45**, 459–462.

ZHURAVLEV, A. Yu., GÁMEZ VINTANED, J. A. and IVANTSOV, A. Y. 2009. First finds of problematic Ediacaran fossil *Gaojiashania* in Siberia and its origin. *Geological Magazine*, **146**, 775–780.